UNLIMITED
UNCLASSIFIED

ILLIMITÉ
NON CLASSIFIÉ

Technical Report

Rapport technique

1984/05

TR-WE-42
NRC No. 23488
TDC No. TP 5346E

# ESTABLISHMENT OF QUANTITATIVE WEAR AND FATIGUE MODEL FOR RAILWAY RAIL SUBJECTED TO HEAVY TRAFFIC CONDITIONS AND DIFFERENT LUBRICATION REGIMES

J. Kalousek

Division of
Mechanical Engineering

Division de
génie mécanique

National Research Council Canada
Conseil national de recherches Canada

Canada

CA1
DTC 845
84
E76
c.2

## DIVISION OF MECHANICAL ENGINEERING PUBLICATIONS

**DM** **(Division of Mechanical Engineering Report)**
Scientific and technical information considered important, complete and a lasting contribution to existing knowledge.

**TR** **(Technical Report)**
Information less broad in scope but a substantial contribution to existing knowledge.

**CTR** **(Controlled/Classified Technical Report)**
A Technical Report with controlled distribution for national security, proprietary or other reasons.

**LM** **(Laboratory Memorandum)**
Preliminary or exploratory information with controlled distribution.

**CAT** **(Calibration Analysis and Test Report)**
Information on minor laboratory projects or services.

## PUBLICATIONS DE LA DIVISION DE GÉNIE MÉCANIQUE

**DM** **(Rapport de la Division de génie mécanique)**
Informations scientifiques et techniques jugées importantes, complètes et susceptibles de contribuer de façon durable à l'avancement des connaissances courantes.

**TR** **(Rapport technique)**
Informations de moindre importance, mais pouvant contribuer substantiellement à l'avancement des connaissances actuelles.

**CTR** **(Rapport technique à diffusion contrôlé/classifié)**
Rapport technique à diffusion contrôlée pour des raisons de sécurité nationale, de propriété intellectuelle et autres.

**LM** **(Mémoire de laboratoire)**
Informations préliminaires ou de nature exploratoire à diffusion contrôlée.

**CAT** **(Rapport d'étalonnage d'analyse et d'essai)**
Informations sur de petits projets ou des services de laboratoire.

UNLIMITED
UNCLASSIFIED

ILLIMITÉ
NON CLASSIFIÉ

Library and Information Centre / Centre de Documentation (GSLA)
RECEIVED – REÇU LE
AUG 21 1984
Transport Canada / Transports Canada

# ESTABLISHMENT OF QUANTITATIVE WEAR AND FATIGUE MODEL FOR RAILWAY RAIL SUBJECTED TO HEAVY TRAFFIC CONDITIONS AND DIFFERENT LUBRICATION REGIMES

Progress Report
Oct. 82 to Sept. 83

**J. Kalousek**

Sponsor Organizations:

Transport Canada
Transportation Development Centre
Montreal, Canada

and

Association of American Railroads
Technical Research Center
Chicago, U.S.A.

1984/05

TR-WE-42
NRC NO. 23488
TDC NO. TP 5346E

Dr. C. Dayson, Head
Division of Mechanical Engineering
Vancouver, B.C., Canada
V6R 1P5

Mr. E.H. Dudgeon
Director/Directeur

The contents of this report reflect the views of the contractor, and not necessarily the official views or policies of the Transportation Development Centre of Transport Canada.

# REPORT DOCUMENTATION FORM

| 1. Transport Canada Report No. | 2. TDC Project No. | 3. Recipient's Catalogue No. |
|---|---|---|
| TP 5346E | 4830 | |

| 4. Title and Subtitle | 5. Report Date |
|---|---|
| Establishment of Quantitative Wear and Fatigue Model for Railway Rail Subjected to Heavy Traffic Conditions and Different Lubrication Regimes - Progress Report October 1982 - September 1983 | May 1984 |
| | 6. Performing Organization Report No. |
| 7. Author(s) | 8. Transport Canada File No. |
| Dr. J. Kalousek | D1465-366-2 |
| 9. Performing Organization Name and Address | 10. DSS File No. |
| National Research Council of Canada (NRC)<br>Western Laboratory<br>3904 West 4th Avenue<br>Vancouver, B.C. V6R 1P5 | 11. DSS or Transport Canada Contract No.<br>4830 |
| 12. Sponsoring Agency Name and Address | 13. Type of Report and Period Covered |
| Transportation Development Centre (TDC)<br>1000 Sherbrooke Street West<br>Suite 2421<br>Montreal, Quebec H3A 2R3 | Technical; Oct.'82-Sept.'83 |
| | 14. Sponsoring Agency Code<br>TDC 4830 |
| 15. Supplementary Notes | 16. TDC Project Officer |
| This is a cooperative project between the Transportation Development Centre and the Association of American Railroads | D.W. Dibble |

17. Abstract

Development of a wear and fatigue model for railway rail has progressed in several areas. Firstly, the wear and contact fatigue resistance of several materials was evaluated on the rail/wheel wear apparatus by means of specifically designed test procedures. Both rail steels taken from as-rolled rails and experimentally developed steels were investigated. Dry wear results compared favourably with those obtained at the Facility for Accelerated Service Testing (FAST). Counts of surface crack initiation sites and fatigue cracks were made in order to assess the material's resistance to contact fatigue. The progress achieved in manufacturing the tribometer and developing its electronic controls is discussed next. Thirdly, an Electron Microscope (EM) investigation of the deformed structure of wear particles was made at the Technical University of Nova Scotia. This work will continue on samples with a richer content of white etching wear particles in order to determine their metallurgical phase. Finally, an analytical and experimental analysis of the contact geometry between the wheel flange and gauge side of the rail was completed. It is described in the attached NRC Technical Report, TR-WE-41.

| 18. Key Words | 19. Distribution Statement |
|---|---|
| Wheel, Rail Wear, Fatigue, Interaction, Wear Particles, Lubrication, Tribometer, Tribology, Metallurgy, Contact Geometry | Limited number of copies available from the Transportation Development Centre |

| 20. Security Classification (of this report) | 21. Security Classification (of this page) | 22. No. of Pages | 23. Price |
|---|---|---|---|
| Unclassified | Unclassified | 50 | --- |

TDC/CDT 79-005

## FORMULE DE DOCUMENTATION POUR RAPPORT

| 1. N° du rapport Transports Canada | 2. N° de l'étude — CDT | 3. N° de catalogue du destinataire |
|---|---|---|
| TP 5346E | 4830 | |

| 4. Titre et sous-titre | 5. Date du rapport |
|---|---|
| Establishment of Quantitative Wear and Fatigue Model for Railway Rail Subjected to Heavy Traffic Conditions and Different Lubrication Regimes - Progress Report October 1982 - September 1983 | mai 1984 |
| | 6. N° du rapport de l'organisme exécutant |

| 7. Auteur(s) | 8. N° de dossier Transports Canada |
|---|---|
| Dr. J. Kalousek | D1465-366-2 |

| 9. Nom et adresse de l'organisme exécutant | 10. N° de dossier — ASC |
|---|---|
| Conseil national de recherches Canada<br>Laboratoire de l'ouest<br>3904 ouest, 4ième avenue<br>Vancouver, B.C. V6R 1P5 | 11. N° de contrat — ASC ou Transports Canada<br>4830 |

| 12. Nom et adresse de l'organisme parrain | 13. Genre de rapport et période visée |
|---|---|
| Centre de développement des transports (CDT)<br>1000 ouest, rue Sherbrooke<br>Suite 2421<br>Montréal, Québec H3A 2R3 | Technique; oct.'82-sept.'83 |
| | 14. Code de l'organisme parrain<br>CDT 4830 |

| 15. Remarques additionnelles | 16. Agent de projet — CDT |
|---|---|
| Ceci est un programme de recherche conjoint, parrainé par le Centre de développement des transports et Association of American Railroads | D.W. Dibble |

17. Résumé

L'élaboration du modèle mathématique figurant le processus d'usure et de fatigue des rails a bien progressé sous plusieurs aspects. D'abord, la résistance d'un certain nombre de métaux a été déterminée à l'aide d'un appareil de mesure de l'usure roue-rail et de méthodes d'essai spécialement étudiées. La recherche a porté tant sur des aciers à rail courants que sur des aciers spéciaux expérimentaux. Les données résultant des essais sur l'usure en régime sec se comparent favorablement à celles obtenues au circuit d'essai FAST.* La résistance à la fatigue de contact des aciers a été déterminée en comparant le nombre d'apparitions de fissures superficielles à celui des fissures développées. Le rapport traite ensuite de l'avancement du tribomètre et de sa commande électronique. Troisièmement, il traite de la recherche faite à la Technical University of Nova Scotia à l'aide du microscope électronique à balayage sur les changements de la structure métallurgique des particules d'usure. Ces travaux doivent se poursuivre sur des échantillons à teneur plus élevée en particules provenant des zones blanches dont il reste à déterminer la phase métallographique. Enfin, le rapport décrit la recherche analytique et expérimentale faite sur la géométrie du contact entre le boudin et la face intérieure du rail (voir annexe "Rapport technique TR-WE-41" du CNR).

* Facility for Accelerated Service Testing

| 18. Mots-clés | 19. Diffusion |
|---|---|
| Usure roue-rail, fatigue, interaction, particules d'usure, lubrification, tribomètre, tribologie, métallurgie, géométrie du contact | Le Centre de développement des transports dispose d'un nombre limité d'exemplaires |

| 20. Classification de sécurité (de ce rapport) | 21. Classification de sécurité (de cette page) | 22. Nombre de pages | 23. Prix |
|---|---|---|---|
| non-classifié | non-classifiée | 50 | --- |

CDT/TDC 78-005

## ACKNOWLEDGEMENT

The financial support provided by the Transportation Development Centre (Canada) and the Association of American Railroads, towards the research projects described in this report, is most gratefully acknowledged.

## EXECUTIVE SUMMARY

The National Research Council of Canada (NRCC) and the University of Rhode Island (URI) are involved in a joint research program concerned with the development of a wear and fatigue model for railway rail. The aim of this program is to provide more accurate and reliable relationships for track maintenance models than the currently used wear indices. Due to the complexity of rail/wheel interactions and the extensiveness of experimental investigations this complexity calls for, it is envisaged that the proposed research program could be completed in four years.

This second annual progress report describes several tasks which are in progress or were completed at NRCC and its subcontractor, the Technical University of Nova Scotia. The work carried out at URI is described in a separate report.

As stated in the first annual progress report, the wear and contact fatigue life of rails are affected by three distinctive but interrelated sets of parameters: mechanical, metallurgical and rheological. The mechanical parameters include, for example, geometry of contact, contact stresses and creep forces acting at the rail/wheel interface. Grain size, inclusions, chemical composition and resistance of material to plastic deformation fall into the group of metallurgical parameters. The rheological parameters help to define the regime of lubrication, which may be dry (no lubrication), boundary (contaminated or lightly lubricated), or intermittent. These parameters include the chemical composition of the lubricant, its viscosity, roughness of rail and wheel surfaces, and tribochemical reactions between the lubricant and rail or wheel material.

The first section of this annual report describes a test program carried out on the rail/wheel wear apparatus. This program was concerned with the evaluation of wear and fatigue resistance of several materials under a predetermined combination of several lubrication regimes. It was concerned with the interaction of all three groups of variables, i.e. mechanical, metallurgical and rheological. The wear data obtained from the unlubricated (dry) test runs compares favourably with the wear data obtained at FAST for head hardened, fully heat treated, standard rails. The contact fatigue resistance of rail steels was evaluated by comparing the counts of surface crack initiation sites and surface fatigue cracks.

The second section of this report briefly mentions the current state of the development of the tribometer. This tribometer, which should become fully operational by the fall of 1984, will help us to evaluate the effect of rheological parameters on traction creepage curves for spin, lateral and longitudinal directions.

The third section describes the Electron Microscope (EM) investigation of the deformed structure of wear particles. Only the structure of dark etching wear particles was determined. The determination of the metallographical phase of white etching particles, the formation mechanism of which is linked to the initiation of surface

cracks, has yet to be accomplished. To this end, samples with a richer content of white etching particles were supplied to Prof. E.E. Laufer, Technical University of Nova Scotia for further EM studies.

The fourth section of this report, NRC Report No. TR-WE-41, is concerned with the geometry of contact, creepage and friction forces occuring between the wheel flange and gauge side of the rail during the hard flanging or on-flange curving mode. It describes the mechanical variables governing the flange contact in the field and in disc-on-disc simulation of flange contact on either full or small scale rigs.

## SOMMAIRE EXECUTIF

Ceci est le deuxième rapport annuel sur l'état d'avancement du programme de recherche conjoint lancé par le Conseil national de recherches du Canada et l'Université Rhode Island des Etats-Unis. Il s'agit du programme pour l'élaboration d'un modèle mathématique figurant le processus d'usure et de fatigue des rails. Le but poursuivi est de trouver, entre les paramètres utilisés pour programmer l'entretien des voies, des corrélations plus fidèles et plus fiables que les indices d'usure d'utilisation courante. Etant donné la complexité des interactions dynamique roue-rail et l'ampleur des expérimentations à faire, il est prévu que le programme de recherche en question s'étale sur quatre ans.

Ce rapport décrit les nombreuses tâches, en cours ou achevées, réalisées par le CNR et son sous-traitant, la Technical University of Nova Scotia. Quant aux travaux faits par l'Université Rhode Island, ils font l'objet d'un rapport séparé.

Comme le mentionne le premier rapport annuel, la tenue à la fatigue et la résistance à l'usure des rails sont liées à trois groupes de paramètres distincts mais interdépendants. Ce sont les paramètres mécaniques, métallurgiques et rhéologiques. Le premier groupe concerne, entre autres, la géométrie de contact du couple roue-rail, les contraintes développées ainsi que les forces de frottement de glissement aux points de contact roue-rail. Le deuxième groupe comprend la grosseur des grains, les impuretés, la composition chimique et la résistance à la déformation plastique. Quant aux paramètres rhéologiques, ils participent à la définition du régime de lubrification qui peut être nul (glissement à sec), limité (faible lubrification ou présence de contaminants) ou intermittent. Les paramètres pris en compte sont la nature du lubrifiant, sa viscosité, l'état de surface des rails et des roues et enfin les réactions tribochimiques entre le lubrifiant et le rail ou la roue.

La première partie du présent rapport annuel traite des essais faits sur l'appareil destiné à mesurer l'usure des rails et des roues. Ce programme d'essais visait à mesurer la tenue à l'usure et à la fatigue d'un certain nombre de métaux, sous une combinaison prédéterminée de régimes de lubrification, et à vérifier l'interaction des trois groupes de paramètres en jeu: mécaniques, métallurgiques et rhéologiques. Les données résultant des essais d'usure en régime sec (sans lubrifiant) se comparent favorablement à celles obtenues du circuit d'essai FAST concernant des rails standard, traités thermiquement et dont le champignon a été durci. La tenue à la fatigue de contact des aciers à rails a été déterminée en comparant le nombre d'apparitions de fissures superficielles à celui des fissures développées.

La deuxième partie du rapport traite brièvement de l'avancement du tribomètre qui devrait être complètement opérationnel d'ici l'automne de 1984. Grâce à cet appareil, il sera possible de mesurer l'effet des paramètres rhéologiques sur le rapport traction-glissement et de ses composantes axiale, transversale et torsionnelle.

La troisième partie aborde la recherche faite à l'aide du microscope électronique à balayage sur les changements de structure métallurgique des particules d'usure. Seules ont été ainsi observées les particules d'usure correspondant aux zones noires, ou zones de transformation structurales. La recherche n'a pas encore porté sur les particules correspondant aux zones blanches, dont il reste à déterminer la phase métallographique et qui sont à l'origine du mécanisme d'apparition des fissures. A cet égard, des échantillons plus riches en particules provenant des zones blanches ont été remis au professeur E.E. Laufer de la Technical University of Nova Scotia, aux fins d'analyses microscopiques plus poussées.

Enfin, la quatrième partie du rapport, c'est-à-dire le rapport TR-ME-A1 du CNR, traite des géométries de contact et des forces de frottement et de glissement entre le boudin et la face intérieure du rail lors des inscriptions forcées en courbe. Elle décrit les paramètres mécaniques en jeu, tant sur voie qu'en laboratoire de simulation en vraie grandeur ou à l'échelle mettant en oeuvre un banc d'essais sur éprouvettes disques.

## CONTENTS


| | | Page |
|---|---|---|
| | ACKNOWLEDGEMENT | (iii) |
| | EXECUTIVE SUMMARY | (iv) |
| | SOMMAIRE EXECUTIF | (vi) |
| **PART I:** | **RAIL/WHEEL WEAR APPARATUS** | 1-1 |
| 1.0 | Test Procedures | 1-1 |
| 2.0 | Wear Rates | 1-3 |
| | 2.1 Dry Wear | 1-3 |
| | 2.2 Lubricated Wear | 1-4 |
| 3.0 | Contact Fatigue | 1-4 |
| 4.0 | Concluding Remarks | 1-8 |
| **PART II:** | **TRIBOMETER DEVELOPMENT** | 2-1 |
| **PART III:** | **TEM EXAMINATION OF RAIL WEAR DEBRIS** | 3-1 |
| **PART IV:** | **CONTACT GEOMETRY BETWEEN WHEEL FLANGE AND RAIL** *Please refer to content listing on page (4-v) | * |


## TABLES

**PART I: RAIL/WHEEL WEAR APPARATUS**


| | | |
|---|---|---|
| 1 | Type and Chemical Composition of Tested Steels | 1-1 |
| 2 | Summary of Fatigue Crack Density and Length Measurements | 1-6 |

## ILLUSTRATIONS

**PART I: RAIL/WHEEL APPARATUS STUDIES**


| Figure | | |
|---|---|---|
| 1 | Bar Diagram of Wear Rates for Several Lubrication Regimes | 1-9 |
| 2 | Surface and Cross Sectional Appearance of Contact Fatigue Crack at Gauge Corner of High Rail | 1-10 |
| 3a | Inclusion Initiated Fatigue Crack (Test I1-LR) | 1-11 |
| 3b | Possibly Surface Initiated Fatigue CRacks (Test A-LR) | 1-11 |
| 4a | Inclusion Initiated Subsurface Cracks (Test I1-HR) | 1-12 |
| 4b | Absence of Subsurface Cracks in Nodular Iron Specimen (Test G-HR) | 1-12 |
| 5 | Surface Texture of E and I Specimens at the End of Test | 1-13 |


**PART II: TRIBOMETER DEVELOPMENT**


| | | |
|---|---|---|
| 1 | Schematics of the Tri-Axial Tribometer | 2-4 |
| 2 | Photograph of the Tribometer and Its Laboratory Loading Device | 2-5 |


**PART III: TEM EXAMINATION OF RAIL WEAR DEBRIS**


| | | |
|---|---|---|
| 1 | Cross Section of Electro-Deposited Ni with Debris | 3-3 |
| 2 | Light- and Dark- Etching Debris Particles in Ni Electro-Deposit | 3-3 |
| 3 | Debris in Ni Deposit, Electropolished | 3-4 |
| 4 | Polishing Pit at Sand Inclusion | 3-4 |
| 5a | Bright Field TEM Micrograph of Rail Wear Debris Particle | 3-5 |
| 5b | Electron Diffraction Pattern of Field of Figure 5a | 3-5 |
| 5c | Dark Field TEM Micrograph of Rail Wear Debris Particle | 3-6 |


**PART IV: CONTACT GEOMETRY BETWEEN WHEEL FLANGE AND RAIL**

Please refer to the list on page (4-v)

# PART I

# RAIL/WHEEL WEAR APPARATUS STUDIES

# RAIL/WHEEL WEAR APPARATUS STUDIES

## 1.0 TEST PROCEDURES

Using rail/wheel wear apparatus previously described in reference [1] we have evaluated the wear and fatigue resistance of seven commercial and two developmental rail steels.

The manner of heat-treatment or alloying of tested steels and their chemical composition are shown in Table 1.

| Code | Manufacturer | Rail Type | C | Mn | Si | Cr | V | Cb | Mo | Cu | N |
|---|---|---|---|---|---|---|---|---|---|---|---|
| A | - | Standard AREA | .80 | .90 | .20 | | | | | | |
| B | Algoma Steel | Cr | .75 | .65 | .25 | 1.15 | | | | | |
| C | Algoma Steel (experimental heat) | Cr-Mo I | .65 | .95 | .30 | .65 | | | .16 | | |
| D | Russian | Through Hardened | .75 | .90 | .30 | | | | | | |
| E | Sydney Steel | Cr-Si-Cb | .70 | 1.10 | .55 | .80 | | .06 | | | |
| F | Bethlehem Steel | Through Hardened | .80 | .90 | .20 | | | | | | |
| G | Experimental | Nodular Iron | 3.3 | .66 | 2.48 | | | | .28 | .73 | |
| H | Experimental | Cr-V | .80 | .95 | .30 | 1.25 | .3 | | | | 0.017 |
| I | Nippon Steel | Head Hardened | .65 | .90 | .20 | | | | | | |

TABLE 1: TYPE AND CHEMICAL COMPOSITION OF TESTED STEELS

All specimens, with the exception of G and H, were manufactured from the heads of as rolled rails. The G specimens were machined from railway wheel commercially produced by a European wheel supplier. The H specimens were manufactured from laboratory produced small heat of rail steel. Two rail disc specimens from each metallurgy, one experiencing the high rail and the other low rail loading environment, were subjected to the test sequence consisting of four steps:

1. 1st MGT* (40,000 rev's) was run dry. No lubricant was used but the surfaces were contaminated by oxidized wear debris generated during this run.

2. 2nd till 20th MGT (next 760,000 rev's) were lubricated by a mixture of grease (Texaco marathon #3) and quartz sand (20% sand by weight).

3. 21st MGT (from 800,000 till 840,000 revs.) was again run dry.

4. 22nd MGT till 60th MGT (840,000 till 2,400,000 revs.) were lubricated by grease only.

Within each test the angle-of-attack was alternated each 2,500 revs between 10', 18', 36' and 40'. Each 20,000 revolutions the machine was stopped, the direction of disc rotation reversed, and the angles of attack changed from a positive to a negative value to maintain the same orientation of curvature. The load during all the tests was constant at 7,000 N (1,570 lb.) producing a sustained maximum hertzian pressure of 1,800 MPa (261 ksi). Use of such a high level of contact stresses in these tests was necessary to simulate the stresses which occur in the field between the wheel's false flange and field side of low rail, or the wheel's flange root and gauge side of high rail. The rail disc profiles and weights were taken before and after each step. Upon completion of the test run, the rail disc specimens were sectioned, polished and subject to metallographical examination.

The above test parameters were chosen to simulate an 8° curve in a single main line track. The entire test sequence was, and remains, computer controlled. Thus any additional tests, if run by the same computer program, will produce test results comparable to those presented here. A good repeatability of test results is demonstrated by the 1st and 3rd steps performed on identical rail material denoted by "I" in Figure 1. This test had to be repeated since no data were available from the 4th step of the II test run.

Figure 1 indicates the loss of material from high and low rail discs during each step. Above each identifying letter there are two columns. The right column indicates the wear rate from high, and the left column from low, rails respectively. Assuming the wear on the top running surfaces of high and low rail discs is the same the differential in wear rate between right and left columns for dry runs could be attributed to flange wear. In case of lubrication by a grease-sand mixture and by grease only, no distinctive flange wear pattern exists. The rail discs were subject to different wear modes, namely delamination and contact fatigue, resulting in lower wear rates, as indicated by the different wear rate scales on diagrams shown in Figure 1. Let us first discuss in more detail the dry wear and then the lubricated one.

---

* MGT - Million Gross Tons of traffic carried over a section of railroad track. A rail disc in the wear apparatus carries an equivalent of 1 MGT if it is subject to the same number of loading cycles at the same contact stress levels as the rail in the field.

## 2.0 WEAR RATES

### 2.1 Dry Wear

Two MGT's, the first and twenty-first, were subject to dry wear. In both cases the form of wear on the top running surfaces was mild adhesive wear, while in the flange contact, severe adhesive wear (gouging) prevailed. However, larger wear rates were observed in the 21st MGT than in the 1st one. One possible explanation for this phenomenon may be that during the rolling-sliding process in the 1st MGT, a larger portion of dissipated energy went towards the generation of plastic flow and work hardening of the subsurface layers than towards the generation of new surfaces, resulting in the formation of wear particles.

During the 21st MGT run the surfaces were already work hardened and a larger portion of dissipated energy went towards the generation of new particles leading to higher wear rates. The presence of a decarburized layer on newly laid rails and possible differences in contact geometry may, nevertheless, obliterate the observation of this phenomenon in the field. The main purpose of dry runs, however, was to evaluate the resistance of various rail materials to gauge face wear.

The wear resistance of various rail steels can be most conveniently compared with the help of the figure of merit (FM) as introduced by Steele and Reiff [2] and defined as:

$$FM = \frac{\text{average wear rate of standard rail}}{\text{average wear rate of comparison rail}}$$

Figures of merit for the materials tested on the rail/wheel wear apparatus and at FAST under nonlubricated (dry) wear regimes in the gauge face area are as follows:

Wear apparatus: I : F : A ≈ 5.3 : 3.5 : 1 (8° curve)

FAST (coding as per [2]): HH : FHT : Std. ≈ 3.5 : 2.1 : 1 (4° curve)

Due to increased creepages and loads occurring in flange contact in sharper curves, materials exhibited higher wear rates in sharp curves than in shallow ones. In addition, because the method of measuring wear rates differed between FAST and our apparatus, the former utilizing caliper gauges and the latter specimen weighing, the FM of a material with the same wear resistance increased nonlinearly with curvature. Comparison of wear rates was accomplished by prorating one of the figures of merit. Assuming that the simulated 8° curve on the wear apparatus increased, with respect to the 4° curve at FAST, by a factor of 1.6, then the equivalent FM for a 4° curve on the wear apparatus becomes: Wear apparatus: I : F : A ≈ 3.31 : 2.18 : 1 (4° curve prorated)

These figures indicate that the simulation of dry wear on the rail/wheel wear apparatus compares favourably with the controlled full-scale environment. Thus the wear apparatus can predict the resistance to dry wear of any rail steel which is commercially produced or under development.

### 2.2 Lubricated Wear

Lubricant, whether a grease-sand mixture or grease only, was applied to both the gauge face and top surfaces of rail discs. Although we have attempted to lubricate the flange-gauge face contact, these attempts were not successful. Either severe lubrication breakdown occurred at flange contact when the supply of grease was restrained, or, when the grease was supplied in sufficient quantities to prevent such a lubrication breakdown, it migrated to the rail/wheel tread interface.

However, regardless of the manner of lubricant application, the amount of lubricant retained by both flange and tread interfaces was governed by the roughness of the rail/wheel disc surfaces, and the lubricant viscosity and excess lubricant were displaced to the sides of the contact zones. Both lubricant media were contaminated during the course of the test by wear debris.

The sand, crushed by the rail/wheel discs into microscopic particles of the average size of 2.5 μm, imbedded itself into either the rail or wheel material, and abraded the other. Thus as seen in Figure 1(b), either low rail or high rail would wear more depending on the random manner by which the sand was distributed throughout the rail/wheel interfaces. This mild form of abrasive wear, note the difference in scales between Figs. 1a and 1b, was accompanied by the formation of a white etching layer on rail surfaces and delamination wear, as discussed in Reference 3. The implication of this portion of the test to the field conditions is that in lubricated territories where the lack of adhesion has to be enhanced by sanding, the rate of material removal is low and unaffected by the quality of the rail steel. However, the quality of rail material still affects the resistance of material to plastic flow and contact fatigue damage. Also, if a breakdown of lubrication film occurs in the field, the wear rates shown in Figure 1(c), being one order of magnitude larger, will override those generated during lubrication by grease-sand-wear debris mixtures.

The rate of material removal was extremely low when the surfaces were lubricated by grease only. In fact use of the term "wear rate" in this case would be highly misleading since the material was not removed gradually in the form of small particles, but intermittently in the form of much larger flakes. This form of surface damage, to be discussed next, is termed "contact fatigue". Although" lubrication by the grease-sand mixture may be more realistic of field conditions, grease-only lubrication was used to enhance the rate of contact fatigue damage to rail discs and to bring the overall test length to a manageable limit.

## 3.0 CONTACT FATIGUE

Many metals, including steel, are damaged by the repeated application of rolling contact stresses and show initiation and growth of fatigue cracks. In ball or roller bearings the term 'contact fatigue' is used to describe the fatigue processes leading to the development of spalling. Spalling occurs when a piece or fragments of metal suddenly detach from the surface of the roller or racer, thereby terminating the useful life of the bearing. For most of the bearing's life the development of the fatigue crack remains hidden and the location

where the spall occurs is not known. In the case of rail, however, hairline or small cracks can be observed on rail surfaces in the early stages of the rail's life. Further propagation of these and subsurface cracks, to be discussed later, lead to the development of large flakes and spalls on low rail, and shelly spots on high rail, as shown in Figure 2. Contact fatigue in bearings and rails differ more than in just the above aspect. While the failed bearing races exhibit none or minute subsurface plastic flow of metal, the contact fatigue in rails is always associated with severe plastic flow of subsurface metal. Under normal operating conditions the bearings are elastohydrodynamically lubricated with uncontaminated lubricants, but rails when lubricated, experience boundary or starved boundary lubrication. In addition, the rail lubricants become always contaminated by wear debris and other impurities, namely minerals.

It is not known at present if the contact fatigue cracks in rails originate at or below the surface. Since it is well established that both mechanisms of crack initiation exist in ball and roller bearings, where contact fatigue processes were investigated to a much greater depth than in the case of rails, let us assume that both crack initiation processes also exist in rails. The possible mechanism of both processes is described next.

Surface initiation of cracks: Numerous observations made by the author on metallographically polished sections of worn rail heads and rail disc specimens indicate that the surface cracks may be initiated by the crevices brought about by the flattened folds of metal. At first, the individual folds of metal are formed by plastic flow of metal over the cavities or depressions left on the rail surface by delaminated or otherwise removed wear particles. A number of such microscopic folds then coalesce forming a hairline fold oriented in a direction perpendicular to the prevailing direction of surface tractions. (See Figure 2). Due to the high level of contact stresses and friction at the rail/wheel interface, the initial folds of metal are rolled into metal tongues which, in the case of full-scale rail, could become several tenth of a millimeter long. The cavities under these tongues, often filled with a mixture of lubricant and contaminants, then constitute the initiation sites for further propagation of contact fatigue cracks.

Subsurface crack initiation: In pearlitic steels subject to incremental plastic deformation the subsurface cracks can be nucleated by either microvoids or inclusions. Although the origin of voids is not known it has been suggested that the interaction of dislocations and the formation of dislocation forests may be responsible, namely at the subgrain boundaries where the colonies of ferrite/cementite lamella change direction. The voids are of extremely small size, say .1 μm or less. The rail steels contain an appreciable number of inclusions. Those of manganese sulfide or iron sulfide origin are usually larger in size and more frequent than the harder silica or aluminum oxide inclusions. Numerous studies [3,4] have shown that the inclusion initiated cracks are affected by the hardness of the inclusion, the cohesion strength between inclusion and matrix and a stress field surrounding the inclusion. In the case of rail steels, the cyclic elastoplastic shear stresses will, during the process of incremental collapse of the subsurface layer, initiate a crack at the vicinity of the inclusion, regardless of its hardness. An example of such crack formation is shown in Figure 3a.

| Specimen Code | High - H Low - L Rail | Initiation Sites < 60 μm | Cracks > 60 & < 600 μm Count (Av. Length) | Cracks > 600 μm Count (Av. Length) | Total Surface Cracks | Subsurface Cracks Count (Av. Length) | VHN kg/mm$^2$ | Max. Depth of Plastic Deformation |
|---|---|---|---|---|---|---|---|---|
| A | H<br>L | 10<br>11 | 20(215)<br>20(182) | 2(780)<br>3(860) | 66 | 65(43)<br>26(40) | 260 | 480<br>300 |
| B | H<br>L | 14<br>17 | 29(180)<br>13(15) | 2(1,035)<br>- | 75 | 62(33)<br>8(49) | 320 | 390<br>150 |
| C | H<br>L | 9<br>12 | 21(183)<br>25(178) | 2(1,470)<br>- | 69 | 51(39)<br>- | 320 | 390<br>150 |
| D | H<br>L | 13<br>14 | 32(172)<br>31(168) | 1(1,470)<br>- | 91 | 9(58)<br>2(90) | 340 | 360<br>140 |
| E | H<br>L | 36<br>14 | 47(193)<br>29(147) | -<br>- | 126 | 41(45)<br>1(30) | 340 | 380<br>150 |
| F | H<br>L | 23<br>14 | 24(189)<br>14(161) | 1(750)<br>- | 76 | 69(24)<br>21(22) | 370 | 360<br>140 |
| G | H<br>L | 20<br>15 | 16(128)<br>19(103) | -<br>- | 71 | -<br>- | 330 | 90<br>50 |
| H | H<br>L | 14<br>14 | 23(158)<br>18(132) | -<br>- | 69 | 63(31)<br>9(37) | 370 | 360<br>140 |
| I | H<br>L | 8<br>14 | 26(208)<br>36(159) | 2(780)<br>- | 86 | 70(46)<br>- | 370 | 240<br>120 |

TABLE 2: Summary of Fatigue Crack Density and Length Measurements

Once the cracks have initiated they will grow and, as mentioned previously, shorten the rail life due to the development of flakes, spalls and shelly spots. At present no criteria have been developed to quantitatively evaluate the degree of contact fatigue damage in rails. In the field, the degree of acceptable contact fatigue damage may vary considerably, not only between the individual railroads, but also within the subdivisions on any main line track. This may be attributed to the variations in the development rate of contact fatigue damage which is considerably affected by the differences in loading and lubrication environments which are route or even site specific. Since we have tested all the rail specimens under the same test conditions, we propose that the frequency and length of cracks as observed on metallographically polished cross sections of rail discs could provide the means to rate the contact fatigue resistance of tested steels.

Three rail disc cross sections, taken at the same location on each disc with respect to the original rolling direction of the rail, were polished, etched and examined for cracks under an optical microscope. The length of individual cracks were measured. Though we could not determine which cracks were surface, void or inclusion initiated, we made an assumption that all cracks shorter than 60 μm were in fact crevices or surface crack initiation sites. We also noted that cracks larger than 600 μm reached the boundary between the plastically deformed layer and the underlying undeformed steel. When the material located above such cracks broke off by ductile fracture, a large spall appeared on the surface of the specimen. Since the service life of rails is terminated upon the occurrence of deep shelly spots or spalls, the growth of cracks into undeformed material is undesirable. It is assumed that the specimens which developed the large (> 600 μm) cracks would fail in contact fatigue earlier than those in which the cracks remained confined to the plastically deformed layer. We have also noted the frequency and length of all subsurface cracks, an example of which is shown in Figure 4a. An inclusion was observed at the center of many of these cracks. The results of crack frequency and length measurements for all crack categories are shown in Table 2. This table also shows the base hardness of tested steels and the maximum depth of the plastically deformed layer measured at the gauge corner of a high rail and the field side of a low rail disc specimen.

Review of Table 2 shows that the G specimens have, with respect to all other specimens, a distinctly superior resistance to contact fatigue. The G specimens were machined from nodular iron, the microstructure of which consists of a bainitic matrix containing graphite nodules. Though the base hardness of the G specimens lies in the mid-range of pearlitic steels, the maximum depth of their plastically deformed layer is only about one third as thick. Both high and low rail disc specimens showed low counts of short cracks. As shown in Figure 4b the subsurface cracks did not form.

The fatigue resistance of pearlitic steels is more difficult to evaluate. Good correlation was obtained between the base hardness of steel and the maximum depth of the plastically deformed layer. Steel I showed the lowest depth of the plastically deformed layer, but the number and length of observed cracks lay in mid-range of those observed in other steels. However, the shelling was not evident on the disc surfaces, see Figure 5a. Steel E on the other hand exhibited the lowest

number of subsurface cracks but it had the largest number of cracks less than 600 μm long. The high incidence of cracks was accompanied by mild shelling, namely on the high rail disc as shown in Figure 5b. Though the plain carbon steel A did not exhibit extensive cracking in a range below 600 μm, it showed the most frequent occurrence of cracks larger than 600 μm and the thickest plastically deformed layer in both high and low rails. Yet, steel D showed the lowest count of subsurface cracks, but the crack count below 600 μm was on the high side with one of the cracks propagated deep into undeformed material.

The above observations indicate that the technique of crack length measurement, though in some ways promising, cannot be used in its present form to conclusively rate the contact fatigue resistance of pearlitic rail steels. The contact fatigue processes within the plastically deformed material appear, in many aspects, to be subject to a larger number of influencing factors than the processes leading to dry wear. It is particularly desirable to expand the above technique, for example, by quantitative analysis of the type, size and density of inclusions. A more detailed analysis of surface and subsurface contact stresses, including the effect of friction at the surface and within the crack cavity on the initiation and propagation contact fatigue cracks is also desirable.

## 4.0 CONCLUDING REMARKS

The laboratory studies described above have attempted to rate the rail steels by their resistance to wear and contact fatigue. The dry wear tests correlate rather closely with the controlled full-scale wear tests. Since, at present time, no other techniques to evaluate the development or progression of flaking and shelly spots seem to exist, the measurements of crack lengths on metallographically polished cross sections of rail discs were used as a first step in our effort to evaluate the contact fatigue resistance of rail steels.

## REFERENCES


1. Kalousek, J. "Rail/Wheel Wear Testing Facility". NRCC-DME Transportation Newsletter, Vol. 13, No. 1, July 1981.

2. Steele, R.K. Reiff, R.P. "Rail: Its Behaviour and Relationship to Total System Wear". Proceedings of the FAST Engineering Conference, 1981, Report No. FRA/TTC-82/01.

3. Hoo, J.C. "Rolling Contact Fatigue Testing of Bearing Steels". ASTM STP 771 (1982).

4. Suh, N.P. "Surface Interactions in the Tribological Technology". Edited by P.B. Senholzi, Martinus Nijhoff Publishers, 1982, pp. 37-208.

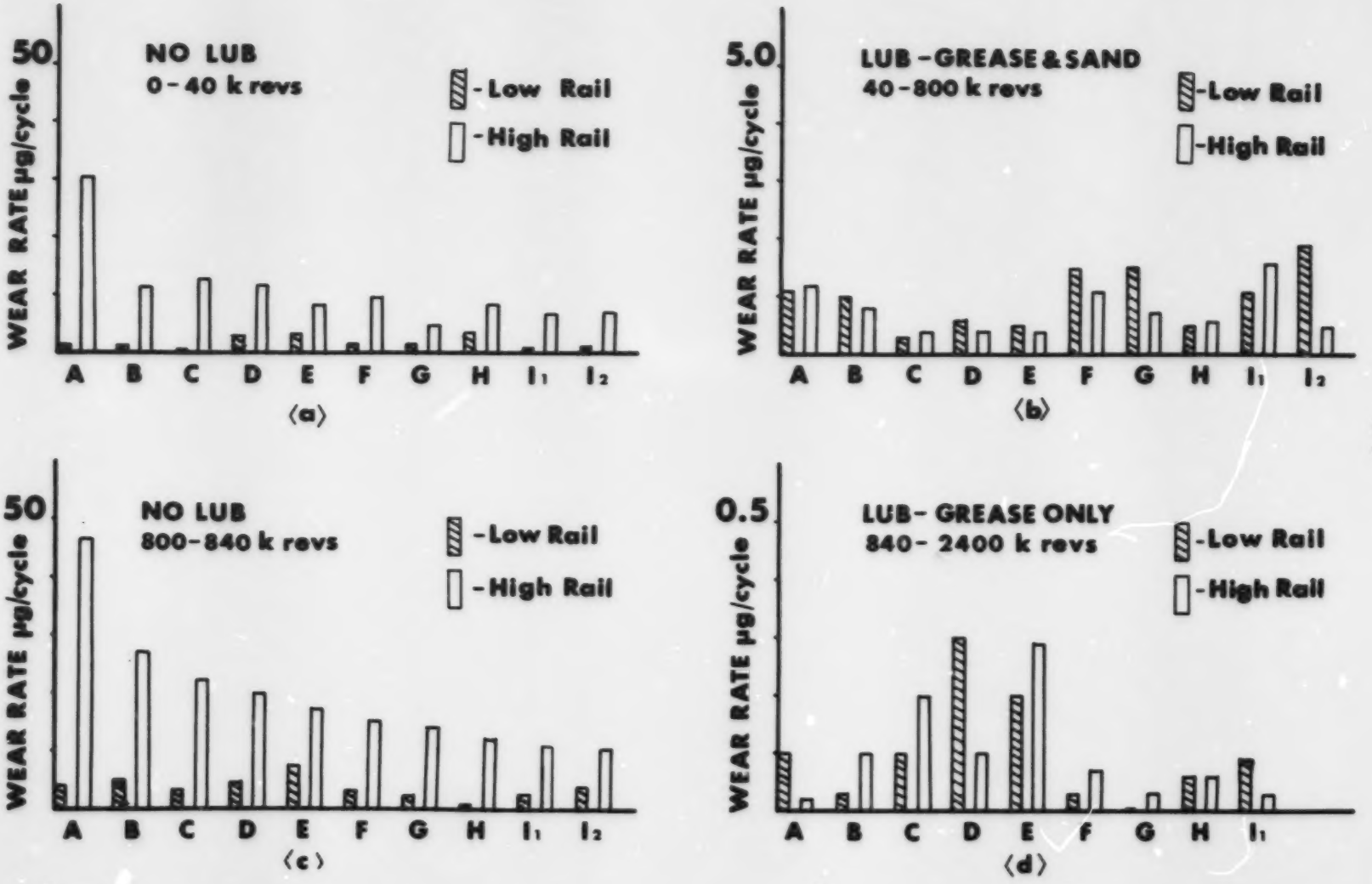


FICURE 1: Bar Diagram of Wear Rates for Several Lubrication Regimes

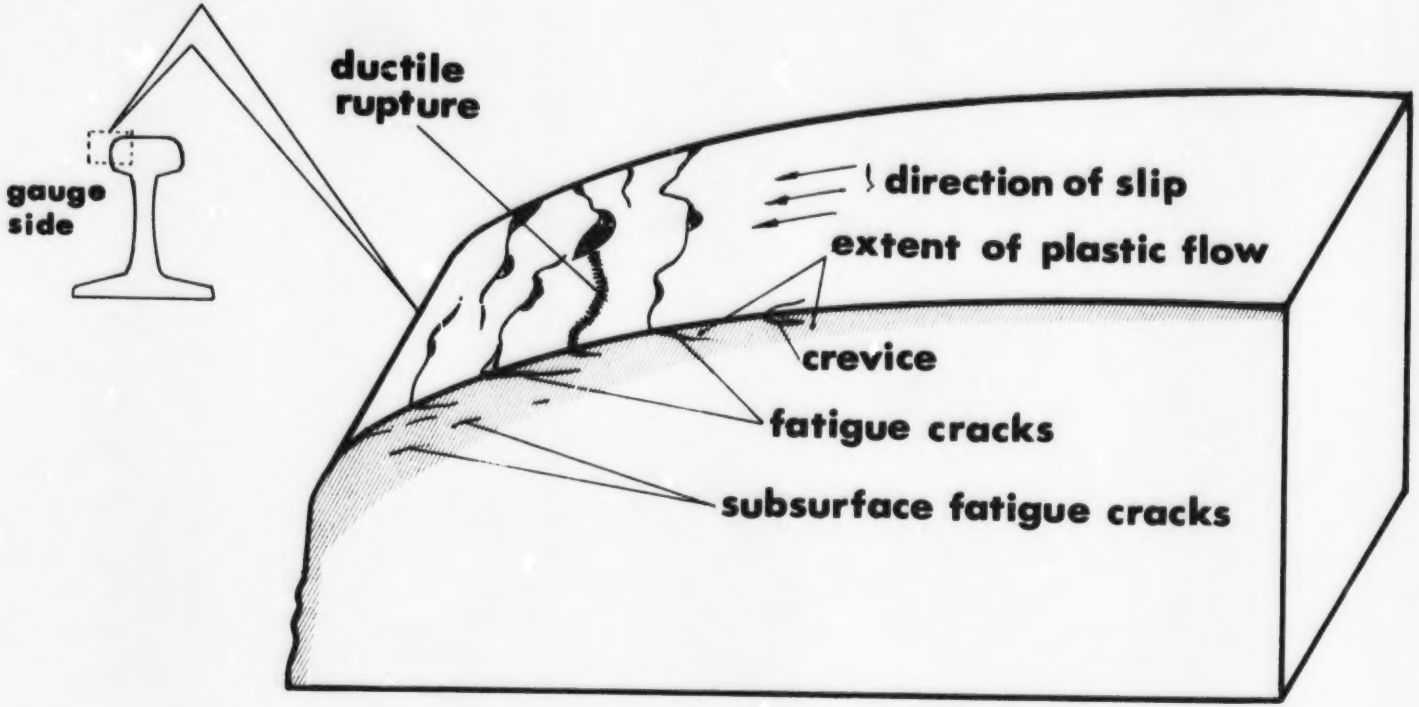


FIGURE 2: Surface and Cross Sectional Appearance of Contact Fatigue Cracks at Gauge Corner of High Rail

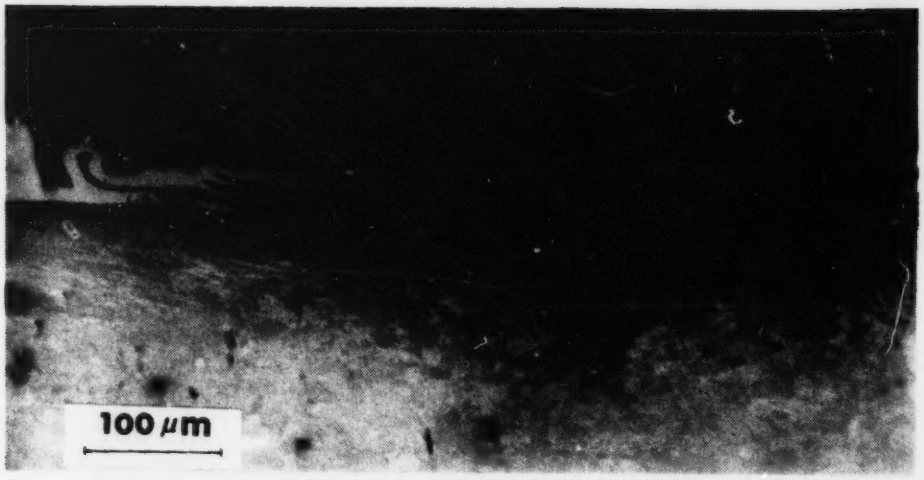


a) Inclusion initiated fatigue crack (Test I1-LR)

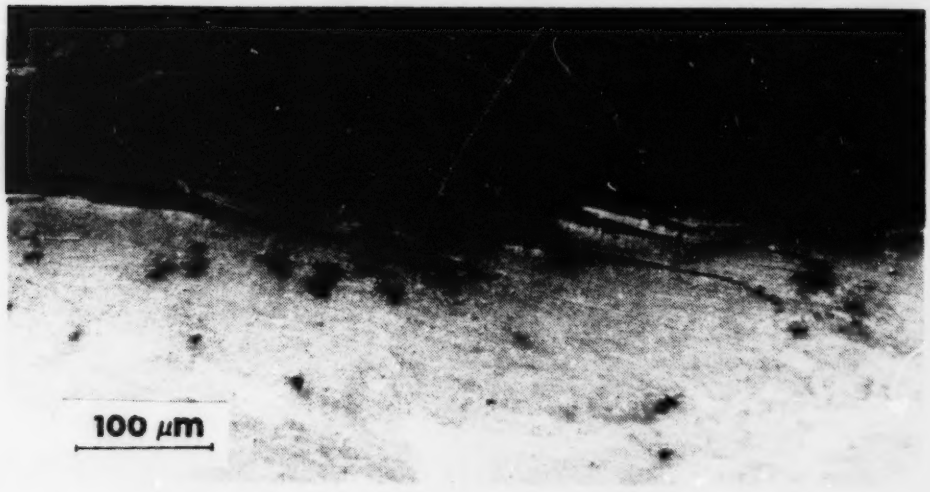


b) Possibly surface initiated fatigue cracks (Test A-LR)

FIGURE 3

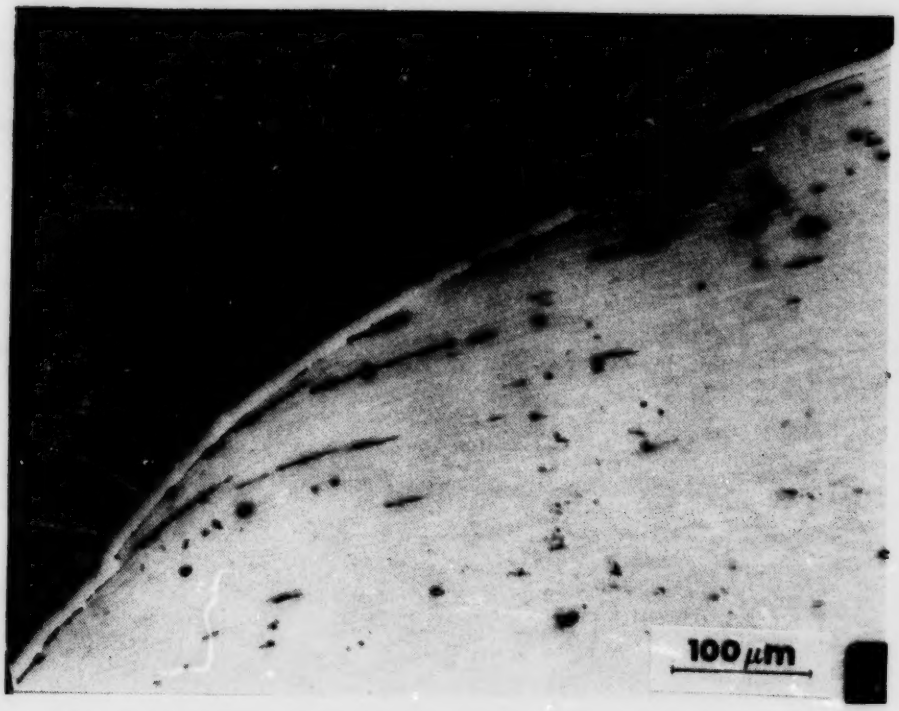


a) Inclusion initiated subsurface cracks (Test I1-HR)

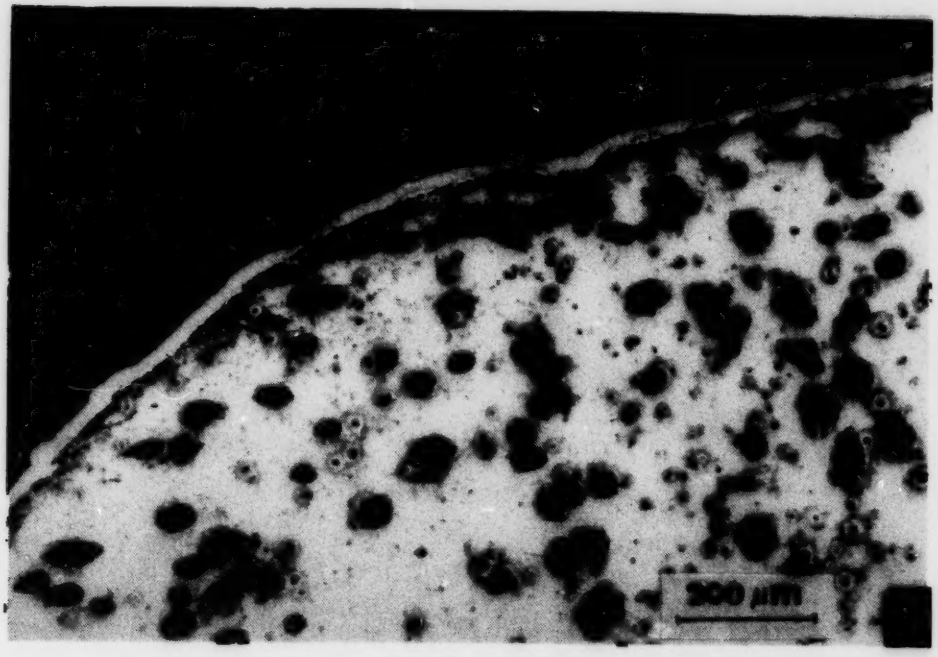


b) Absence of subsurface cracks in nodular iron specimen (Test G-HR)

FIGURE 4

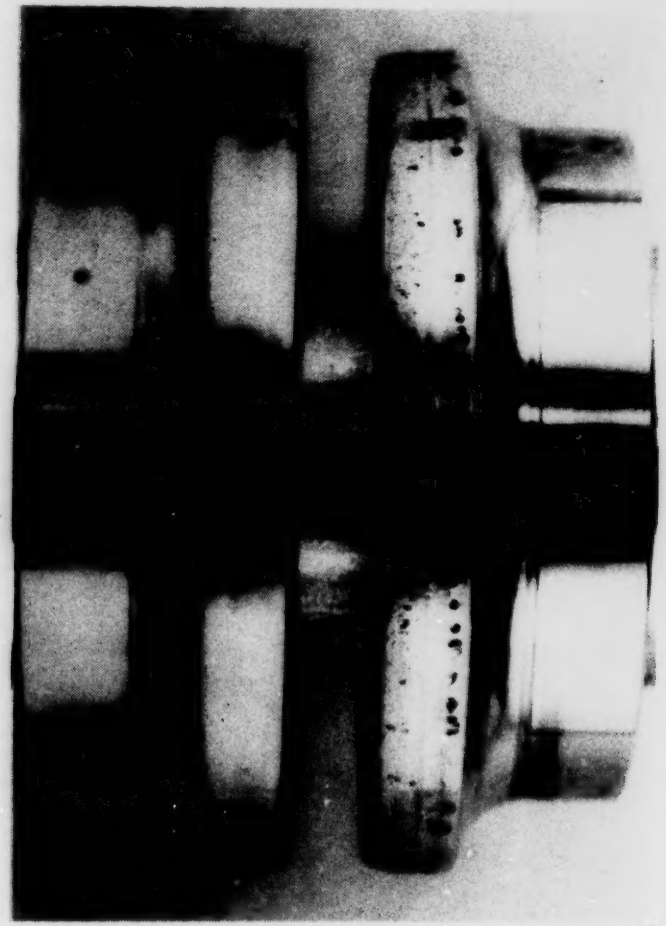

a) E Specimens

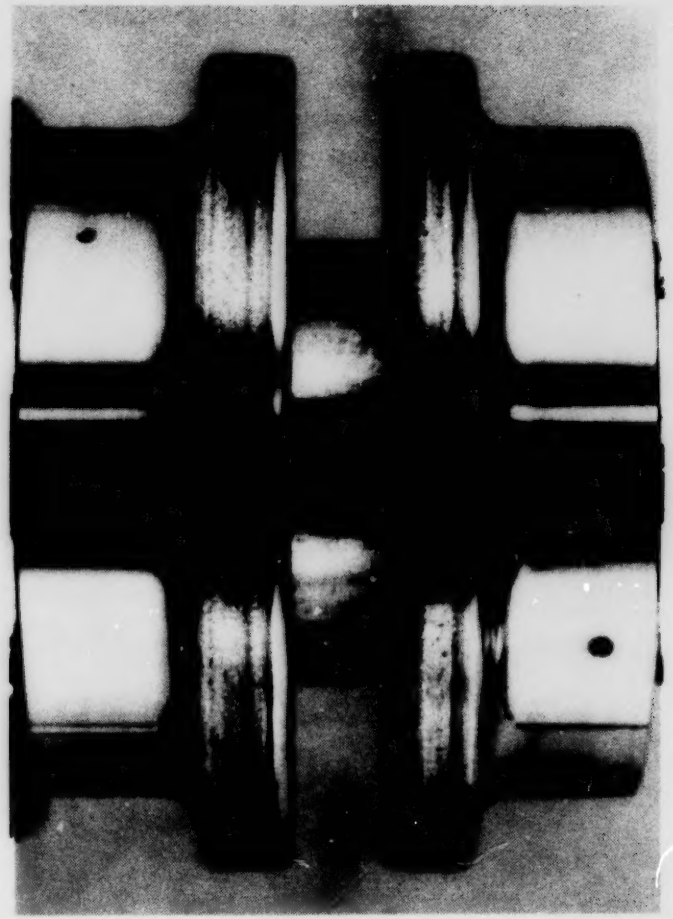

b) I Specimens

FIGURE 5: Surface Texture of E and I Specimens at the End of Test.
Note the spalls on the HR of E Specimen.

# PART II

# TRIBOMETER DEVELOPMENT

## TRIBOMETER DEVELOPMENT

The term 'tribometer' is used to describe an instrument capable of measuring any traction force-creepage relationship in rolling sliding contact. Such relationships affect the steering behaviour of vehicles, the amount of material removed from the rail/wheel interface by wear processes, the rate of plastic flow of subsurface layers of rail or wheel materials as well as the rate of propagation of contact fatigue cracks. For the dry surfaces with Coulomb friction these relationships can be calculated theoretically, either for single or any combination of longitudinal, lateral and spin creepages, using, for example, Kalker's computer programs, 'CONTACT' or 'DUVOROL', [1]. For the non-Coulomb friction prevailing between contaminated or lubricated surfaces, Kalker's theory and associated computer programs have to be modified. Any modification of Kalker's or any other theory, however, have to be experimentally validated.

Several small scale laboratory and field tribometers have been designed and built [2-5]. These instruments are able to measure only the single, longitudinal creepage-traction force relationship. British Rail and the Electro-Motive Division of General Motors Corporation instrumented the diesel-electric locomotives to serve as full-scale tribometers again to measure the creepage-traction force relationship for low [6] and high [7] ranges of longitudinal creepage. The 'Decoped Car' built by British Rail [8,9] is a full-scale lateral tribometer. It measures lateral creepage-traction force relationships which have the most pronounced effect on the steering behaviour of freight car trucks in curves. The tribometer, currently under development at the Western Laboratory, is a small-scale instrument designed to simultaneously measure or evaluate the effect of longitudinal, lateral and spin creepages on the traction force vector at the rail/wheel interface.

Our tribometer is designed for both laboratory and field use. In a laboratory environment it can be used to experimentally validate Kalker's modified theory or any other theory attempting to predict the traction creepage relationship in contaminated or lubricated rolling sliding contacts. The field generated data produced by this tribometer can assist the railroads in studying the efficacy of track side mounted lubricators (or lubricants), and in generating reliable input data for steady state curving or hunting computer programs. It could also help establish the adhesion limits available to individual trucks within the consist of locomotives.

The cut out isometric view of the tribometer is shown in Figure 1. It consists of two 8" dia. wheels, one to measure traction forces on the interface and the other to establish the velocity of 'free-rolling' in the field. The measuring wheel could be electromagnetically braked, mechanically misaligned in yaw by ± 3° to generate lateral creepage and it could also be tilted by ± 30° to generate spin. The tribometer's instrumentation permits the measurement of vertical and lateral loads, and torque and spin moments acting on the measuring wheel. These last three parameters can be plotted with respect to either lateral, longitudinal or spin creepages, or any combination of these parameters. To carry out laboratory measurements the tribometer is equipped with a loading device (see Figure 2) which could accomodate the rail or wheel discs from the Rail/Wheel Wear Testing Apparatus.

An Apple II microcomputer with appropriate interface modules and recording device will give commands to, and record the data generated by, the tribometer. At the time of writing, the computer program is still being developed. It is envisaged that the instrument will be fully operational by the fall of 1984.

## REFERENCES


1. Kalker, J.J. "Introduction to the Fortran IV programs, DUVOROL and CONTACT, for the solution of 3D elastostatic half-space contact problems with or without friction". Report of the Department of Mathematics and Informatics, No. 82-29, Delft University of Technology, 1982.

2. Collins, A.H. Pritchard, C. "Recent Research on Adhesion". Railway Engineering Journal, Sept. 1972, pp. 19-34.

3. "Manually Operated Tribometer". Railway Gazette International, June 1982, p. 463.

4. Andrews, H.I. "Chemical Methods of Improving Rail Adhesion". Proc. Instn. Mech. Engrs., Vol. 178, 1964, Pt. 3E, pp. 172-184.

5. Wambold, J.C. Popjoy, M.A. "Development of a Field Tribometer for Railroad Use". The Pennsylvania Transportation Institute Report No. PT I 8205, Pennsylvania State University, March 1982.

6. Watkins, D.J. "Exploring Adhesion with British Rail's Tribometer Train". Railway Engineering Journal, July 1975, pp. 6-13.

7. Longston, C.F.Jr. Itami, G.S. "Locomotive Friction-Creep Studies". ASME Paper No. 80-RT-1.

8. Pocklington, A.R. "The BR Load Measuring Wheel". Proceedings of the International Symposium on Wheel/Rail Load and Displacement Measuring Techniques, Cambridge, Massachusetts, 1981, U.S. Dept. of Trans., DOT-TSC-UMTA-82-3, pp. 4-1 - 4-29.

9. Pearce, T.G. Rose, K.A. "Tangential Force-Creepage Relationships in Theory and Practice". Contact Mechanics and Wear of Rail Wheel Systems, University of Waterloo Press, 1983, pp. 183-196.

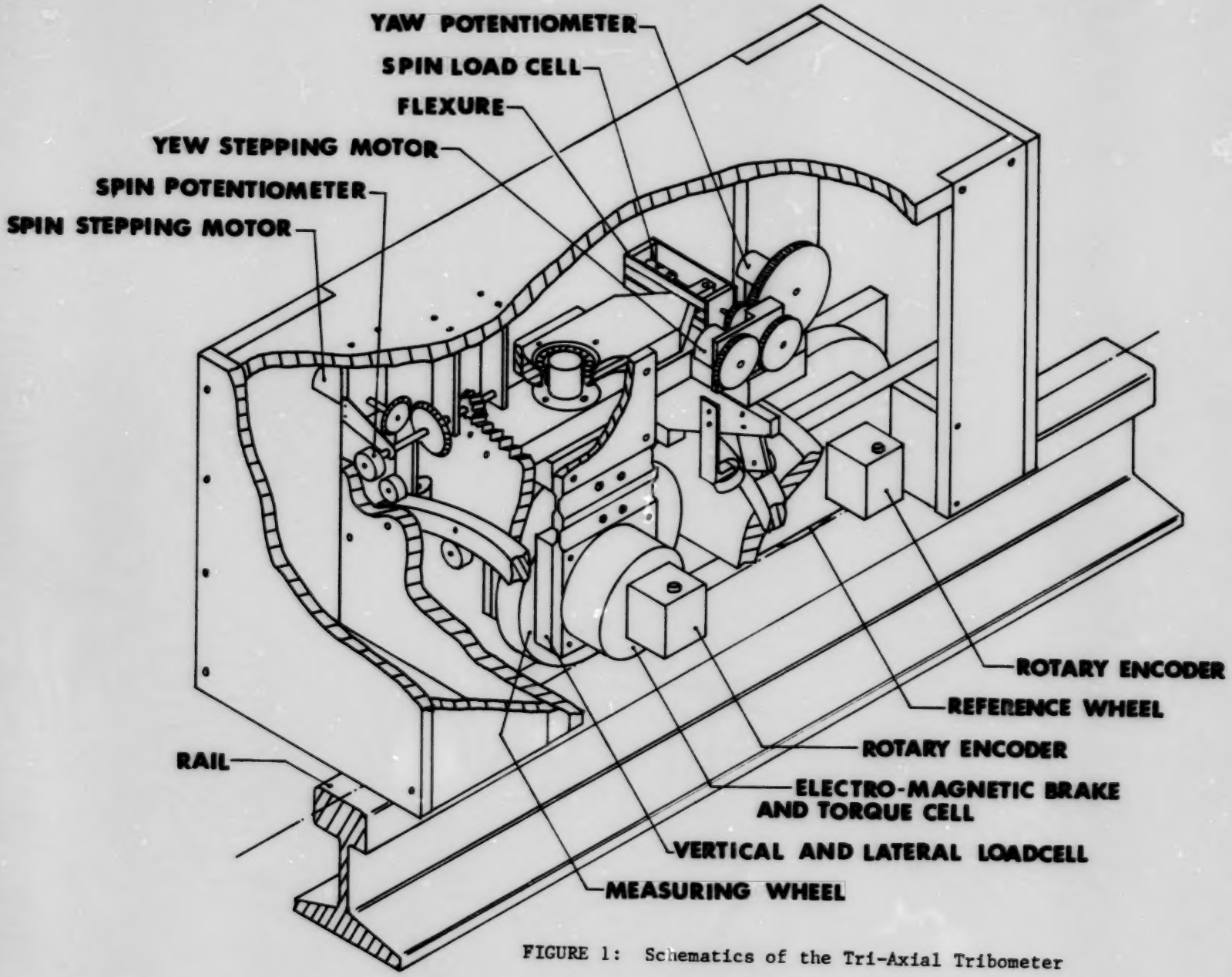


FIGURE 1: Schematics of the Tri-Axial Tribometer

FIGURE 2: Photograph of the TRIBOMETER and its Laboratory Loading Device

# PART III

## TEM EXAMINATION OF RAIL WEAR DEBRIS

## TEM EXAMINATION OF RAIL WEAR DEBRIS

(Reported by Prof. E.E. Laufer, Technical University of Nova Scotia)

The objective of this project was to prepare and examine TEM (Transmission Electron Microscope) samples of rail wear debris, and especially to identify 'white etching' particles.

A number of preliminary and intermediate objectives were defined:

i) Determine whether we can distinguish between rail wear and wheel wear debris.

ii) Support rail wear particles for TEM sample preparation.

iii) Prepare TEM samples.

iv) Identify white-etching particles.

These problems have been dealt with as follows:

i) A sample of premium rail containing about 1% Cr was examined in the SEM, together with a sample of standard rail. Using energy dispersive X-ray spectroscopy (EDS), the 1% Cr sample was easily distinguished from the other. Thus, if debris particles come from premium rail/wheel interaction or any system where there is a similar difference in chemical composition, the particles can be identified by EDS.

ii) To support the particles for TEM examination, they were incorporated into a Ni electrodeposit as follows:

- a brass substrate was prepared by evaporating a carbon parting layer onto one surface.
- cleaned debris particles were held against the carbon coated layer by a magnet on the opposite face.
- the substrate, with particles, was plated to give a sample whose cross section was as shown in the micrograph, Figure 1.

The Ni plating with particles could then be separated from the substrate and mechanically ground and polished to produce a flat sheet about 100 μm in thickness. Etching this sheet revealed light- and dark-etching particles (Figure 2).

iii) TEM samples have been prepared by:

- cutting discs, 1.5 mm dia., by electro-erosion. The discs are cut from regions of the Ni sheet, which contain white-etching debris particles.

- electro-polishing the discs in a modified commercial jet-polishing unit ('Metalthin'). Polishing is stopped automatically when a perforation first occurs in the disc.

A successfully prepared TEM sample will have a perforation at or very near a debris particle of interest, and the metal around the perforation, including all or part of the debris particle, will be thin enough to be transparent to electrons, i.e., less than about 500 μm. Two types of experimental difficulty limit the number of successful samples. Firstly, the location of the perforation, which normally occurs near the center of a disc, is not controllable. Continued electro-polishing leads to a perforation with thick, opague edges. Thus, there is an element of chance in 'hitting' a debris particle. Secondly, perforation may occur due to preferential attack at any point, e.g., a dirty debris-Ni interface, sand or other non-debris particles, improper polishing conditions leading to preferential attack of either the Ni or the debris. Figures 3-5 illustrate the difficulties and success to date.

Figure 3 shows a debris particle as electropolished in the Ni sheet. The plating interface is good, and slight preferential polishing of the particle is not likely to cause difficulty. Figure 4 shows perforation at a pit, caused by entrapped sand. Figures 5a, b and c show some of the first TEM micrographs obtained. Figure 5a shows microstructure in bright field. Figure 5b shows a diffraction pattern of the region of 5a. The rings are due to ferrite and/or martensite, which are difficult to distinguish by electron diffraction, and indicate a very fine grain size. Figure 5c is a dark field micrograph of a region adjacent to that shown in 5a. Each individual bright region represents a separate grain, and graphically illustrates the exceedingly fine grain structure produced in the debris particles.

The investigation is continuing with preparation and examination of new samples.

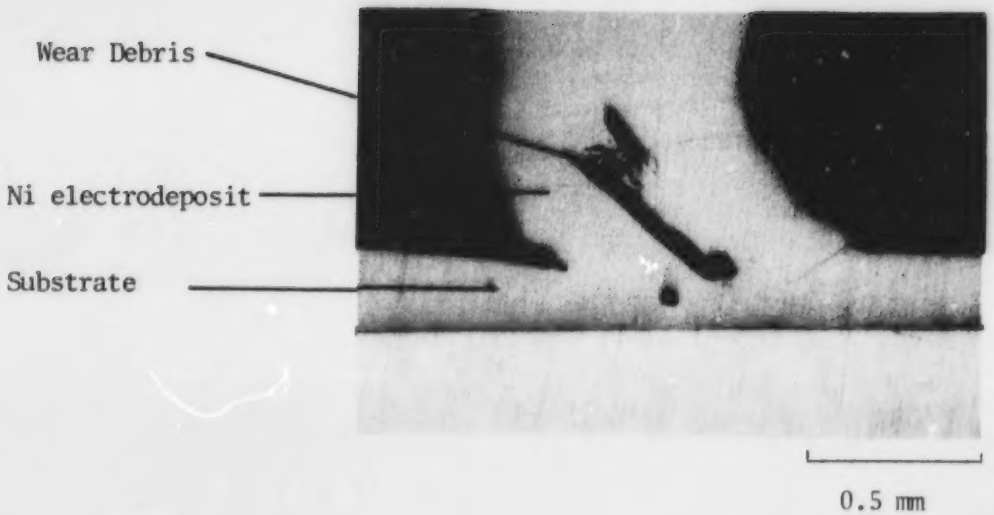


FIGURE 1: Cross section of electro-deposited Ni with debris.

FIGURE 2: Light- and dark-etching debris particles in Ni electro-deposit.

10 µm

FIGURE 3: Debris in Ni deposit, electropolished

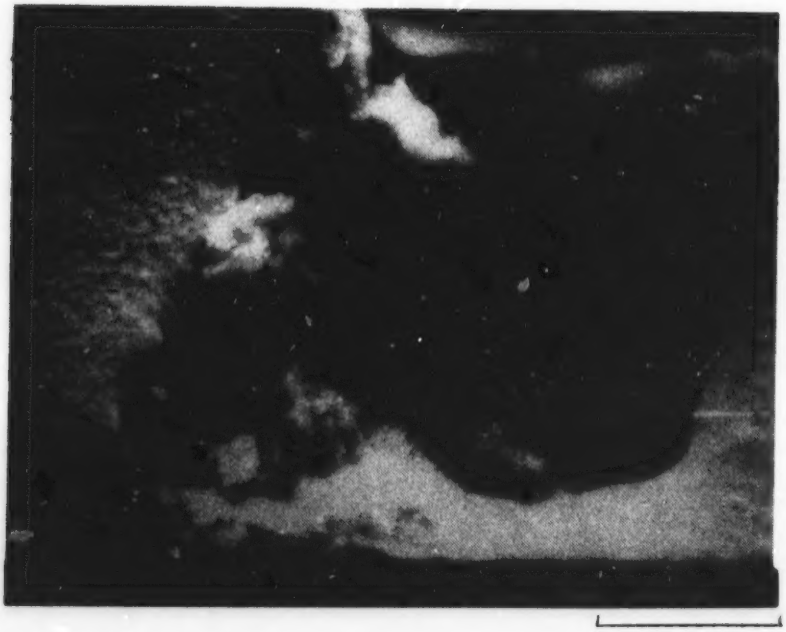

10 µm

FIGURE 4: Polishing pit at sand inclusion

FIGURE 5a: Bright field TEM micrograph of rail wear debris particle.

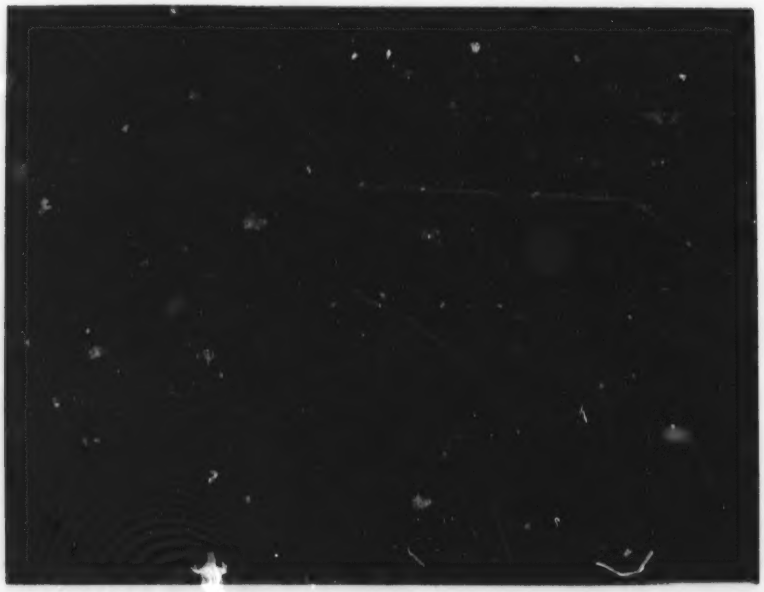

FIGURE 5b: Electron diffraction pattern of field of Figure 5a.

FIGURE 5c: Dark field TEM micrograph of rail wear debris particle.

# PART IV

## CONTACT GEOMETRY BETWEEN WHEEL FLANGE AND RAIL

UNLIMITED
UNCLASSIFIED

ILLIMITÉ
NON CLASSIFIÉ

# CONTACT GEOMETRY BETWEEN WHEEL FLANGE AND RAIL

# GEOMETRIE DE CONTACT ENTRE LE BOUDIN DE LA ROUE ET LE RAIL

J. Kalousek

Division of Mechanical
Engineering Report

1984/03

Rapport de la Division
de Génie Mécanique

TR-WE-41
NRC NO. 23208

Dr. C. Dayson, Head
Division of Mechanical Engineering
Vancouver, B.C., Canada
V6R 1P5

Mr. E.H. Dudgeon
Director/Directeur

**ACKNOWLEDGEMENT**

This report describes a portion of a broad rail/wheel wear research program which has been undertaken jointly by the Western Laboratory and the University of Rhode Island. The financial support of the Transportation Development Centre (Canada) and the Association of American Railroads towards this program is greatly appreciated. The author also expresses his gratitude to Mr. H. Ackroyd for his excellent technical assistance and to Mrs. K. Fassler for meticulous typing of the manuscript.

**ABSTRACT**

This report is concerned with contact between the conical section of a wheel flange and the flat portions of the gauge side rail between wheel and straight rail and wheel and disc rail. Experimental observations strongly support the theoretical analyses of contact geometry, slippages and frictional flange force.

**RÉSUMÉ**

Le contact entre la section conique du boudin d'une roue et la portion plate du côté intérieur d'un rail est décrit pour les cas expérimentaux effectués en laboratoire et sur les rails.

Les observations expérimentales supportent avec force les analyses théoriques de la géométrie du contact, du phénonène de glissement et de la force tangentielle de frottement du boudin de la roue.

## NOMENCLATURE

| | |
|---|---|
| $a, b$ | major and minor semiaxis of flange contact ellipse |
| $e_x$, $e_z$ | longitudinal and vertical distance between contact points B and C |
| $h$ | distance between two mesh points within the contact area |
| $r_c$ | wheel flange radius at point C |
| $r'_c$, $r''_c$ | rail and wheel disc radii at point C |
| $r_{hor}$ | radius of curvature at point C in a horizontal plane parallel to the wheelset axis |
| $r'_{hor}$, $r''_{hor}$ | rail and wheel disc horizontal radii at point C |
| $r_w$, $r_r$ | wheel and rail disc radii at contact point B |
| $R'$, $R''$ | rail and wheel radii normal to contact zone |
| $l$, $c$ | subscripts denoting longitudinal and cross-sectional planes normal to contact zone |
| $V_i$ | slip speed vectors at individual mesh points |
| $\alpha$ | semiapex angle of wheel flange conical section |
| $\beta$ | angle between gauge side of rail and a wheelset axis |
| $\gamma$ | angle of wheel's rotation |
| $\Delta s$ | length of streak or wear mark left by a wheel asperity on a side of rail |
| $\psi$ | angle-of-attack (yaw angle of wheelset with respect to track centerline) |
| $\omega$ | angular speed of a wheelset |

## CONTENTS


| | | Page |
|---|---|---|
| | ACKNOWLEDGEMENT | (ii) |
| | ABSTRACT | (iii) |
| | NOMENCLATURE | (iv) |
| 1.0 | INTRODUCTION | 1 |
| 2.0 | THEORETICAL CONSIDERATIONS | 1 |
| | 2.1 Wheel and Straight Rail | 1 |
| | 2.2 Wheel and Disc Rail | 3 |
| 3.0 | EXPERIMENTAL VERIFICATION OF CONTACT GEOMETRY | 4 |
| 4.0 | SLIPPAGE | 4 |
| 5.0 | FLANGE FRICTION FORCE | 6 |
| 6.0 | CONCLUSIONS | 7 |
| | REFERENCES | 9 |


## ILLUSTRATIONS


| Fig. | | |
|---|---|---|
| 1 | Flange Contact Between Wheel and Rail | 10 |
| 2a | Rail/Wheel Contact Geometries Leading to Elliptical Flange Contacts | 11 |
| 2b | Radii of Curvature of Normal and Horizontal Conical Sections at C | 11 |
| 3a | Advancement of Flange Contact Caused by Yaw Misalignment | 12 |
| 3b | Advancement of Flange Contact for Wheel/Rail Disc Apparatus | 12 |
| 4 | Change in Longitudinal Distance Between Tread and Flange Contact Zones as Function of Angle-of Attack | 13 |
| 5 | Theoretical and Measured Advancement of Flange Contact Point | 14 |
| 6 | Flange Contact Impressions With Varying $\alpha$ and $\beta$ | 15 |
| 7 | Generation of Prolate Cycloid | 16 |
| 8 | Distribution of Slip Vectors Within the Flange Contact | 17 |
| 9 | Flange Force Vector and Its Orthogonal Components | 18 |

# CONTACT GEOMETRY BETWEEN WHEEL FLANGE AND RAIL

## 1.0 INTRODUCTION

Curving of freight car truck wheelsets can occur in two modes: off-flange and on-flange. During off-flange curving the forces between the wheelset and rails are transmitted through two zones of contact. Though the wheel flange can be in close proximity to the high rail there is no contact. The contact area on the high rail is nevertheless displaced towards the gauge side and is characterized by high conicity. The wheel tread tractions can be determined analytically using the theory of Johnson and Vermeulen [1], sometimes preferred for its simplicity, or by using one of Kalker's several algorithms [2,3], which take more computing time but are more exact. Numerous computer programs have been developed, validated and are currently being used to evaluate the quasi-static or dynamic behaviour of off-flange curving.

During on-flange curving the forces between the wheelset and rails are transmitted through three contact zones: two between the wheel and high rail, and a third between the other wheel and low rail. Although the solutions for the contact zones between wheel treads and rail surfaces are analytically well understood and experimentally validated, the same can not be stated about flange contact. Fortunately, flange contact is less complex than wheel tread/rail surface contact. This is due to the fact that flange contact is subject to sliding only and does not contain any locked-in region as is the case with tread contacts.

This report attempts to summarize the analysis of flange contact including geometry, slip distances and frictional forces. It is hoped that it will benefit those involved in on-flange curving analysis, rolling resistance in curves, wear or derailment studies and simulation of wheel or wheelset behaviour on roller rigs.

## 2.0 THEORETICAL CONSIDERATIONS

### 2.1 Wheel and Straight Rail

Hard flange contact occurs between the conical section of the wheel flange profile and the gauge side of the rail. The conical section is typically 7 mm (≈ 1/4") wide on new wheels. This width can increase with wear up to 30 mm (1 1/4"). The flange cone angle, $\alpha$, also increases with wear from 70° up to over 80°. The flange cone contacts the upper gauge corner of the rail, if it is new, or the flat section of the gauge side of the rail, if it is worn. Thus the problem of flange contact can be reduced to the study of contact between conical and flat surfaces as shown in Figure 1.

The height of the contact point, $e_z$, is determined from the geometry of the wheelset contacting a pair of rails. To do this, it is necessary to consider not only the shape of rail and wheel profiles but also their mutual orientation. The value, $e_z$, reaches its maximum when the inclination of the gauge side plane, $\beta$, is smaller than the cone angle, $\alpha$, as shown in Figure 2a. For $\alpha < \beta$ the $e_z$ reaches its minimum and the contact occurs in the vicinity of the flange root.

$\alpha = \beta$ yields a line contact typical of a conical section contacting a flat plane. The length of this contact is, however, severely limited by the lesser height of either the rail's gauge side or the wheel's conical surfaces. The $e_z$ in this case should be measured with respect to the centre of this line contact.

The forward displacement of the flange contact point, $e_x$, can be determined as a function of the angle-of-attack. Sectioning the flange cone in a horizontal plane yields a parabola of radius of curvature, $r_{hor}$, at its vertex (see Figure 2b) which is given by the equation:

$$r_{hor} = r_c \, tg\alpha \tag{1}$$

Rolling the vertex of this parabola over the straight side of a rail by a small angle-of-attack, $\psi$, will yield the displacement of contact point, C, (See Figure 3a), by an amount calculated as follows:

$$e_x = r_{hor} \sin\psi = r_c tg\alpha \sin\psi \tag{2}$$

This relationship was first derived by Bodecker [4] and has been used since by many scientists [5 - 8]. It should be pointed out that the worn flanges, say with $\alpha = 78°$, will result in larger $e_x$ than new wheels with $\alpha = 70°$, due to an increase in $r_{hor}$. For the 38" diameter wheel this increase amounts to 71%.

The quantities, $e_x$ and $e_z$, determine the location of the contact point, which becomes the centre of the contact ellipse or the line contact. The dimensions of the contact ellipse or the appropriate section of the line contact are governed by the geometry of the flange and the gauge side of the rail in the immediate vicinity of the contact point. Knowing load and material properties of rail and wheel steels, these dimensions can be calculated using Hertz' theory [9,10]. For the case of $\alpha > \beta$ (See Figure 2a, b) the principal radii are:

$$R''_1 = r_c \sec\alpha; \quad R''_c; \quad R'_1 = \infty; \quad R'_c = \infty \tag{3}$$

For the case $\beta > \alpha$, the principal radii are:

$$R''_1 = r_c \sec\alpha; \quad R''_c = \infty; \quad R'_1 = \infty; \quad R'_c \tag{4}$$

where the values of $R''_c$ and $R'_c$ are determined from the cross-sections of respective rail and wheel profiles under consideration. Since $R''_c$ and $R'_c$ cannot attain large values, the contact ellipse for $\alpha \neq \beta$ will always be rather narrow with its large axis oriented in the longitudinal direction. Such a narrow contact ellipse exhibits small contact area and high contact pressures with a maximum in the range of 500,000 to 800,000 psi.

The line contact geometry at $\alpha = \beta$ is calculated from Hertzian theory applicable to cylindrical contacts [11] taking

$$R''_1 = r_c \sec\alpha \text{ and } R'_1 = \infty \tag{5}$$

Since the length of this contact is limited by the lesser height of the gauge side plane or flange cone it could be appreciably smaller than the contact width. Since the cylindrical contacts generally exhibit larger contact areas than elliptical flange contacts, the contact pressures are appreciably reduced, but can still be high enough to bring about a severe form of adhesive wear.

### 2.2 Wheel and Disc Rail

In many small or full-scale laboratory studies of rail/wheel contact phenomena, the rails are simulated by discs. In order to compare the flange contact data generated in the field with those generated on the disc-on-disc simulator it is necessary to know the distance, $e_z$ and $e_x$, in both situations.

The vertical depression of the flange contact point, $e_z$, is determined in the same manner as in the wheel, straight rail situation. The advancement of the contact point, $e_x$, is generated by rolling the parabola vertexes of the appropriate conical wheel and rail disc sections over each other by a small angle, $\psi$, as indicated in Figure 3b, i.e.:

$$e_x = \frac{r'_{hor}}{r'_{hor} + r''_{hor}} \; e_{xo} = \frac{r'_{hor}\, r''_{hor}}{r'_{hor} + r''_{hor}} \; \sin\psi \qquad (6)$$

For most of the experiments carried out on the disc-on-disc simulator, the rail and wheel discs, unless changed frequently, wear into similar, highly conformal profiles. In particular, the slope of the gauge side of the high rail and wheel flange cone angle will be the same i.e. $\alpha = \beta$ and Equation 6 can be written in the form:

$$e_x = \frac{r'_c \cdot r''_c}{r'_c + r''_c} \, tg\alpha \, \sin\psi \qquad (7)$$

Comparison of Equations (2) and (7) indicates that for the same values of $\alpha$ and $\psi$ the disc-on-disc simulation will always generate a shorter $e_x$ than the field situation.

The shape of the contact area is again a segment of a line contact connecting the apexes of the wheel flange and gauge side cones. The principal radii of this cylindrical contact are:

$$R'_1 = r'_c \sec\alpha \quad \text{and} \quad R''_1 = r''_c \sec\alpha \qquad (8)$$

Hertz' theory which is applicable to line contacts may be used to determine the size and distribution of contact pressure within the flange contact area.

## 3.0 EXPERIMENTAL VERIFICATION OF CONTACT GEOMETRY

Using a one tenth scale rail/wheel wear apparatus [12], the contact patches were obtained from tread and flange contacts for both wheel and straight rail as well as wheel and disc rail combinations. New and worn profiles were NC machined onto wheel discs, rail discs and straight segments of rail blanks. These were then polished to yield a clearer resolution of the shape and dimensions of contact patch. Aluminum foil was inserted in the rail/wheel interface and then the discs were loaded. After the impressions were taken, the foil was flattened and the impressions were measured. An example of the impressions for angles-of-attack where $\psi$ = 0°0', 0°30', 1° and 2°, using a wheel with CN 'Profile A' and a straight rail containing new AREA profile, are shown in Figure 4. The tread contact areas are ellipses with an a/b ratio close to one. The a/b ratio for flange contact is in the vicinity of 10.

The distance $e_x$ measured between the centres of the tread and flange contact zones for wheel/straight rail and wheel/disc rail combinations was plotted against the angle-of-attack as shown in Figure 5. In general, good agreement was obtained between calculated and measured values. An exception can be observed between $\psi$ = 0 - 36' in the case of flange contact with straight rail. Apparently the gauge corner of the rail was not touching the conical section of the flange but the flange root adjacent to it, i.e. the condition of $R'_c = \infty$ was not satisfied.

The imprints shown in Figures 6a and 6b were taken with $\alpha > \beta$ and $\alpha < \beta$ respectively. The location of the gauge corner in both cases is indicated by the dotted line. Although the distance from the dotted lines to the center of the flange contact zone does not represent the $e_z$, it does indicate the difference between the two cases considered. Figures 6c and d show the impressions generated by cylindrical flange contact, i.e. when $\alpha = \beta$. The impressions shown in 6c were obtained by using polished disc and straight rail and those shown in 6d were made by using worn wheel and rail discs. Both impressions demonstrate that while the width of the cylindrical contact zone may be appreciable, its length is limited by the size of the conical section of the wheel flange or the flat portion of the gauge side of the rail.

## 4.0 SLIPPAGE

Knowledge of slip vector distribution throughout the contact zone leads to a better understanding of friction and wear processes, rolling resistance and generation of frictional force within flange contact.

Providing the wheel does not slip at point G in a longitudinal direction, point C on the wheel flange will follow the trajectory of a prolate cycloid. Although we are interested only in that portion of the point C trajectory which lies below the rail's top surface, the manner by which the entire prolate cycloid is generated is shown in Figure 7. Analytically, the curve is described by the following parametric equations:

$$x = r_w\gamma - r_c\sin\gamma$$
$$z = r_w - r_c\cos\gamma \qquad (9)$$

Any prolate cycloid or its portion is easily drawn by using the following rule: A line, connecting the generating point C with contact point G, is always normal or perpendicular to the tangent at point C. The tangent itself indicates the instantaneous direction of a velocity vector. When point C is in contact with the gauge side of the rail, the tangent to C also indicates the direction of the slip vector with respect to the rail.

Letting the generating circle roll by an incremental angle of, say, $\Delta\gamma$, it is possible to plot the instantaneous values of slip vectors for a few selected flange contacts. Three examples of slip vectors within the flange contact are shown in Figure 8. Figure 8a shows the slip vectors for the case in which $\alpha > \beta$ and $\psi = 0$. Although flange contact at $\psi = 0$ rarely occurs in the field because it requires large, unbalanced speeds, this case clearly demonstrates that the instantaneous slip vectors within the flange contact are always symmetrical about the centre of the contact ellipse, i.e. point C. The same observation can be made for the other two cases (Figures 8, b & c) which are, of course, more typical examples of contact geometry occuring in the field than case (a). Providing the distance, h, between the two mesh points within the contact ellipse is $h = r_c\sin\Delta\gamma$, we can construct the shape and length of a slip mark or streak left on a side of rail by a wheel asperity by summing up the instantaneous slip vectors along the ellipse's longitudinal axis. Close agreement was obtained between streaks actually observed and those acquired by the above method. Inset photographs in Figure 8 depict the actual slip marks on the gauge side of a rail corresponding to the discussed cases.

The radius of curvature of a streak can be determined analytically using the following formula:

$$R_s = \frac{[r^2_w - 2r_w r_c\cos\gamma + r^2_c]^{3/2}}{r_w r_c\cos\gamma - r^2_c} \qquad (10)$$

$$\text{where } \gamma = \arcsin\frac{e_x}{r_c}$$

The streak length is constrained by either the width of the contact ellipse, 2b, or the length of the cylindrical contact, 2a. Thus:

$$\Delta s = 2b \text{ (ellipse)}$$
$$= \frac{2a\sqrt{e_x^2 + e_y^2}}{r_w\sin\alpha} \text{ (cylindrical contact)} \qquad (11)$$

Since the contact pressures at the edges of elliptical or cylindrical contact zones may be insufficient to produce plastic deformation of a substrate layer of metal, a more realistic estimate of slip distance is obtained when right-hand expressions in Equation 11 are multiplied by 2/3.

The typical slip length values for hard flange contacts, either calculated or measured, lie in the vicinity of 2.5 mm (0.1"). Depending on the misalignments of a particular wheelset the average slip distance in flange contact may be twenty to several hundred times larger than the average slip in tread contact. The unusually large wear rates observed on wheel flanges and sides of high rails in curves must therefore be attributed to long flange contact slip distances which, on the average, are two orders of magnitude larger than those occurring in tread contact.

In a disc-on-disc configuration the trajectory of a wheel asperity with respect to the rail disc is a prolate epicycloid. The same rule which applies to the design of cycloids governs the generation of epicycloids. The parametric equations of a prolate epicycloid are:

$$x = (r_w + r_r)\cos\gamma - r_c\cos\frac{r_w + r_r}{r_w}\gamma$$

$$z = (r_w + r_r)\sin\gamma - r_c\sin\frac{r_w + r_r}{r_w}\gamma \qquad (12)$$

Within the area of flange contact the prolate epicycloid will always exhibit larger curvature than the prolate cycloid. This curvature increases with the decreasing diameter of rail discs. The slip distances may be estimated using Equation 11. Due to a smaller $e_x$ value these become somewhat shorter than those occuring in a wheel, straight rail flange contact, but the flange-tread slip distance ratio still lies in the two order of magnitude range.

## 5.0 FLANGE FRICTION FORCE

The magnitude of friction force in flange contact is given by a product of the friction coefficient and the magnitude of a normal load, and lies in the direction of rubbing or slippage. The load at the flange contact is dependent on a number of parameters, including tread forces at both wheels, external loading environment and truck suspension. As a rule computer programs or measurements are used to arrive at a good estimate of flange loading. In some instances it can reach a value exceeding that of a vertical wheel load.

The only place at which unsaturated or zero slippage could be obtained is at point B where $e_x = e_z = 0$. Because all flange contact points have $e_z > 0$, the flange contact area will always experience saturated slippage. In other words, no portion of the flange contact area, however small, can contain a locked in region in which the

rail and wheel asperities do not move with respect to each other. However, at different locations within the contact zone, asperities will move at different speeds with respect to their underlying rail points. This speed increases with the distance from point B according to the following formula:

$$V_i = \omega\sqrt{e^2_{xi} + e^2_{zi}} \quad i = 1,..,n \tag{13}$$

Thus the rubbing speed of flange asperities is, by a factor of about 15 to 60, smaller than the speed of the train or the wheel's flange periferal speed. The range of rubbing speeds experienced by flange asperities is not sufficiently large enough to affect the value of the coefficient of friction. Therefore, each asperity, whether near or far from B, produces equal friction force under the same contact pressure. Considering the symmetry of contact pressure and the direction of slip vectors with respect to point C, it follows that the direction of a resultant vector obtained by summing up all frictional forces produced by individual asperities (or, equivalently, summing up all traction forces produced within the discretised subregions of the contact area) must be coincident with the slip direction at point C. Therefore the direction of the slip vector at point C is the exact rather than an approximate estimate of the flange force direction. Unfortunately, the magnitude of this force can only be determined as accurately as the estimate of the coefficient of friction. The friction coefficient could change anywhere from 0.05 for well lubricated contacts and smooth surfaces; to 0.3 for contacts experiencing mild adhesive wear; to 0.6 for contacts experiencing gouging wear.

Decomposing the flange force (L) into its orthogonal components, as shown in Figure 9, it can be seen that this force resists the wheel's rotation, $L_x$, increases the flange loading, $L_y$, and unloads the wheel/rail contact point B, $L_z$. The unloading of contact point B is less pronounced in disc-on-disc rail/wheel simulators, for otherwise identical misalignments and external loading environments, than in the field situation. This is caused by the distance, $e_x$, which is always shorter in disc-on-disc than wheel on straight rail arrangements. For the same reason the flange contact in disc-on-disc simulators generates larger rotational resistance than the equivalent field situation. The amount of decrease in wheel unloading or increase in rotational resistance can easily be evaluated if the $e_x$ and $e_z$ values are known for both disc-on-disc and field situations.

## 6.0 CONCLUSIONS

The purpose of this report has been to present a brief, but concise, analysis of flange contact as it occurs between wheels and rails and wheels and discs using simulating apparatuses. It has been shown that:

(i) The flange contact area is either a narrow ellipse oriented in a longitudinal direction, or a cylindrical contact of short length. Its location with respect to tread contact is given by longitudinal and vertical coordinates, $e_x$ and $e_z$. Hertz' theory must be used to determine the ellipse dimensions.

(ii) The slip directions within the zone of contact are determined by the $e_{xi}$ and $e_{zi}$ coordinates of an individual mesh point. The directions and magnitudes of slip vectors are symmetrical with respect to point C.

(iii) The flange force, always generated by saturated slip, takes on the direction of the slip vector at point C. Its magnitude is determined by the magnitude of force normal to the flange contact and rheological environment, prevailing in the flange contact area.

## REFERENCES


1. Johnson, K.L.
   Vermeulen, P.J.
   "Contact of Non-Spherical Bodies Transmitting Tangential Forces".
   Journal of Applied Mechanics, June 1964.

2. Kalker, J.J.
   "Simplified Theory of Rolling Contact".
   Delft Progress Report, Ser. C,1, 1-10, 1973.

3. Kalker, J.J.
   "Introduction to the Fortran IV Programs DUVOROL and CONTACT for the Solution of 3-D Elastostatic Half-Space Contact Problems With or Without Friction".
   Delft University of Technology, Dept. of Mathematics, Report 82-29, 1982.

4. Bodecker, C.
   "Die Wirkung Zwischer Rad und Schiene".
   1887.

5. Muller, C.T.
   "The Railway Wheelset, Kinematics, Geometry of Track Guidance, Guiding Capacity".
   Glasers Annln, Sept. 1953.

6. Matsui, N.
   "On the Derailment Quotient Q/P'".
   Railway Technical Research Institute, Japanase National Railways, 1966.

7. Gilchrist, A.O.
   Brickle, B.V.
   "A Re-examination of the Proneness to Derailment of a Railway Wheelset".
   J. Mech. Eng. Sci., Vol. 18, No. 3, pp. 131-141, 1976.

8. Marcotte, P.P.
   Matheson, K.J.R.
   Young, R.
   "A Practical Model of Rail Vehicle Curve Negotiation".
   Proceedings of the 7th Symposium of the International Association for Vehicle System Dynamics, Cambridge, 1981.

9. Hoersch, V.A.
   Thomas, H.R.
   "Stresses Due to the Pressure of One Elastic Solid Upon Another".
   University of Illinois Bulletin, Vol. 27, No. 24, 1930.

10. Seely, F.B.
    Smith, J.O.
    "Advanced Mechanics of Materials".
    Wiley, pp. 342-378, 1952.

11. Timoshenko, S.P.
    Goodier, J.N.
    "Theory of Elasticity".
    McGraw Hill, 1970.

12. Kalousek, J.
    "Rail/Wheel Wear Testing Facility".
    NRCC Newsletter on Transportation, Vol. 13, No. 1, July 1981.

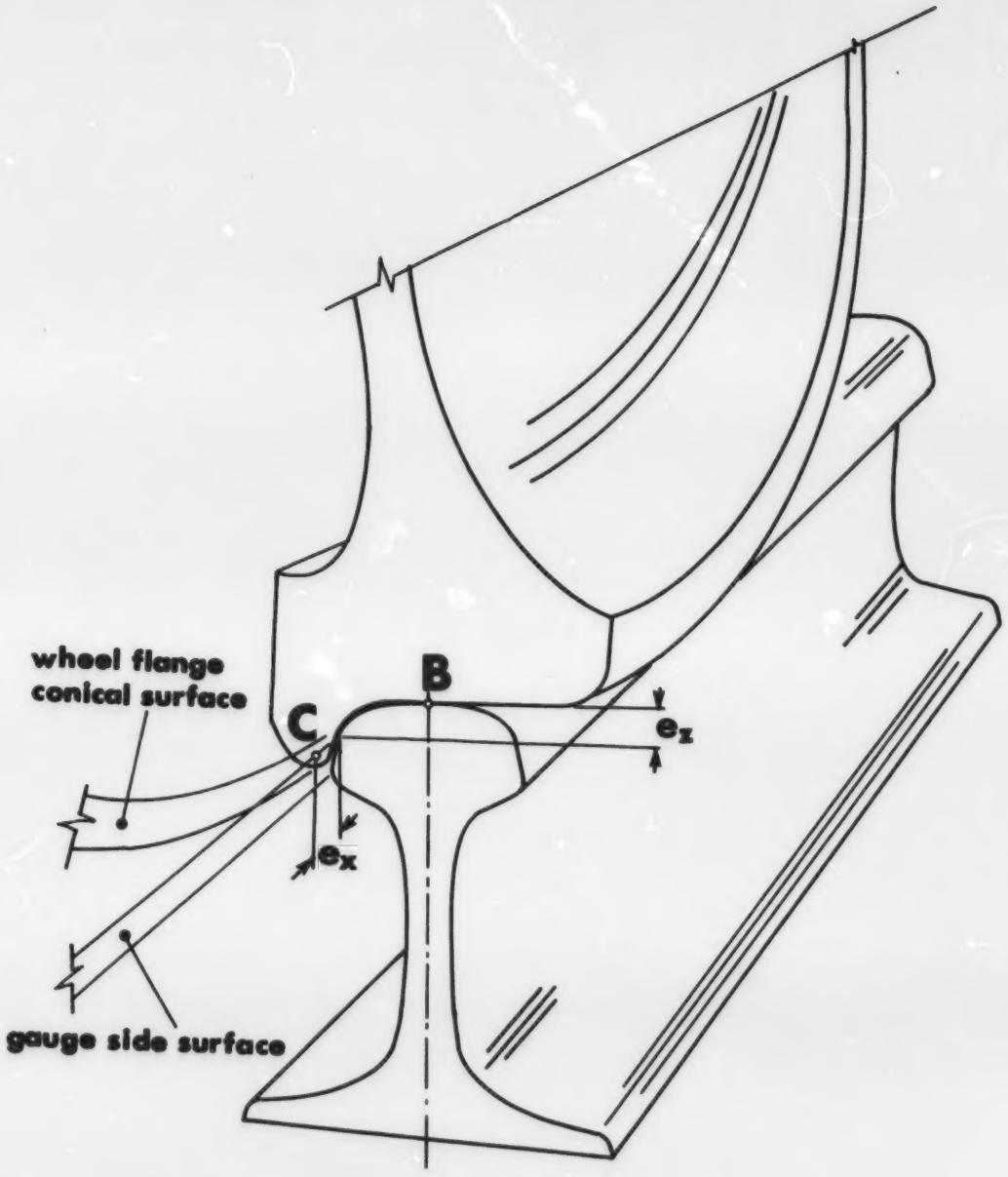


FIGURE 1: Flange Contact Between Wheel and Rail

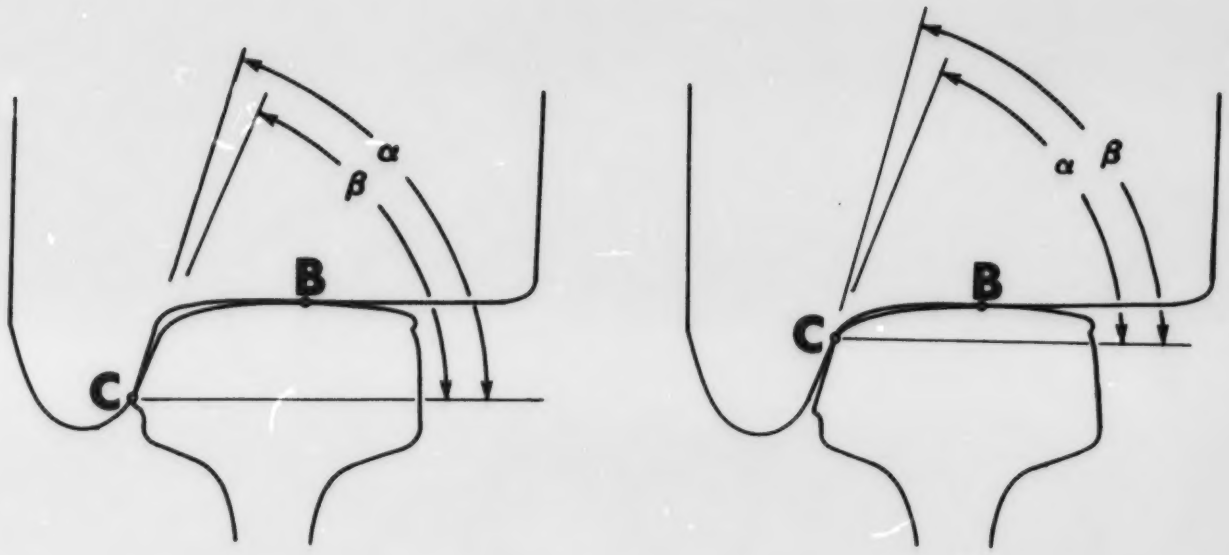


a) Rail/Wheel Contact Geometries Leading To Elliptical Flange Contacts

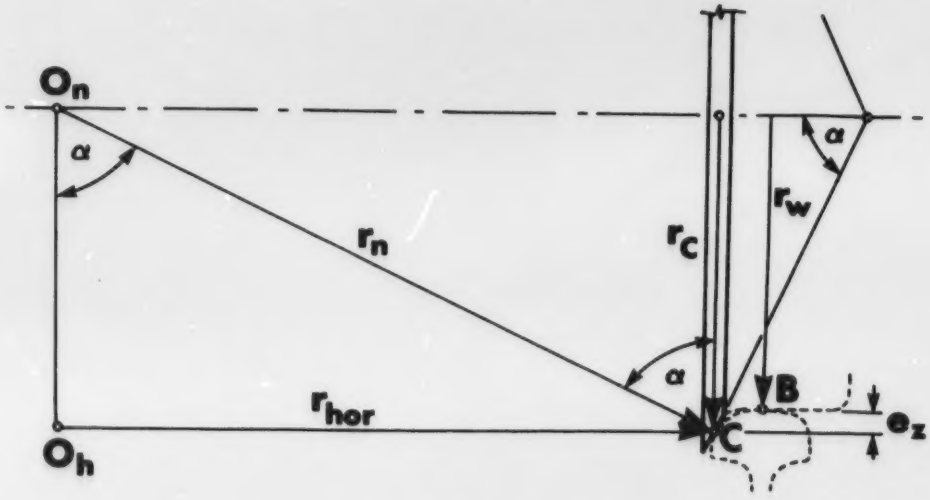


b) Radii of Curvature of Normal and Horizontal Conical Sections at C

FIGURE 2

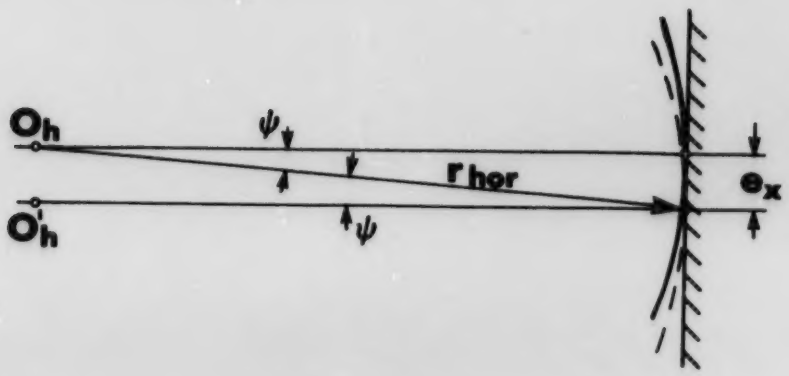


a) Advancement of Flange Contact Caused by Yaw Misalignment of a Wheelset

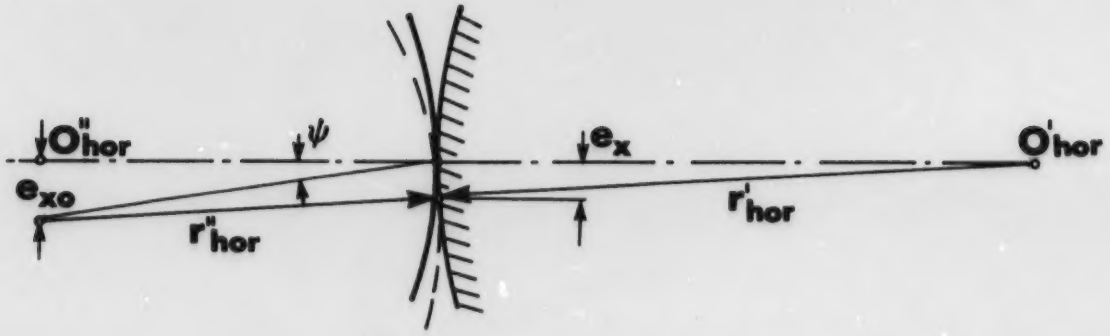


b) Advancement of Flange Contact for Wheel/Rail Disc Apparatuses

FIGURE 3

a) $\psi = 0$

b) $\psi = 30'$

c) $\psi = 60'$

d) $\psi = 120'$

FIGURE 4: Change in Longitudinal Distance Between Tread and Flange Contact Zones as Function of Angle-of-Attack

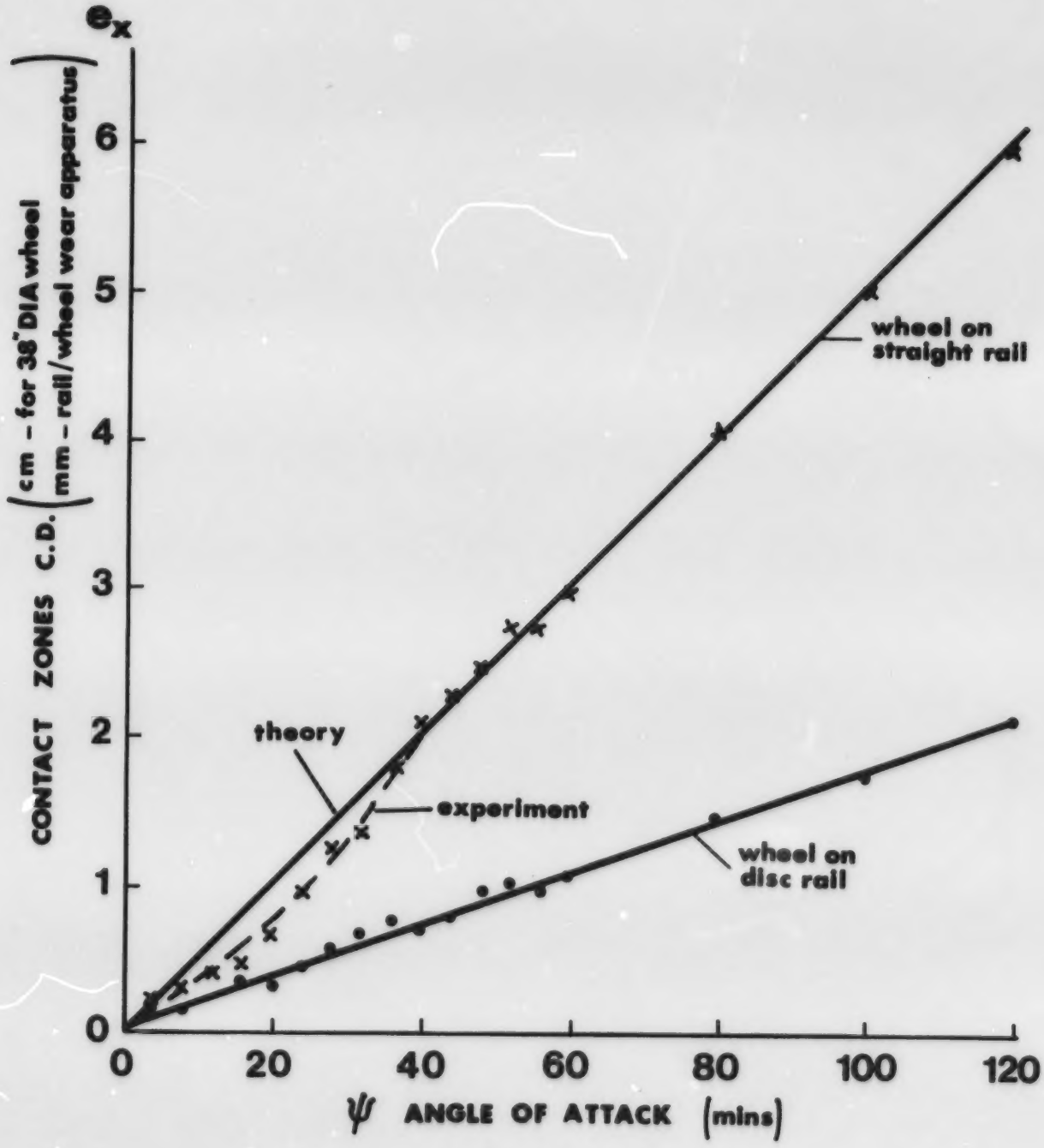


FIGURE 5: Theoretical and Measured Advancement of Flange Contact Point

a) $\alpha > \beta$

b) $\alpha < \beta$

c) $\alpha = \beta$

d) $\alpha = \beta$

**FIGURE 6:** Flange Contact Impressions With Varying $\alpha$ and $\beta$

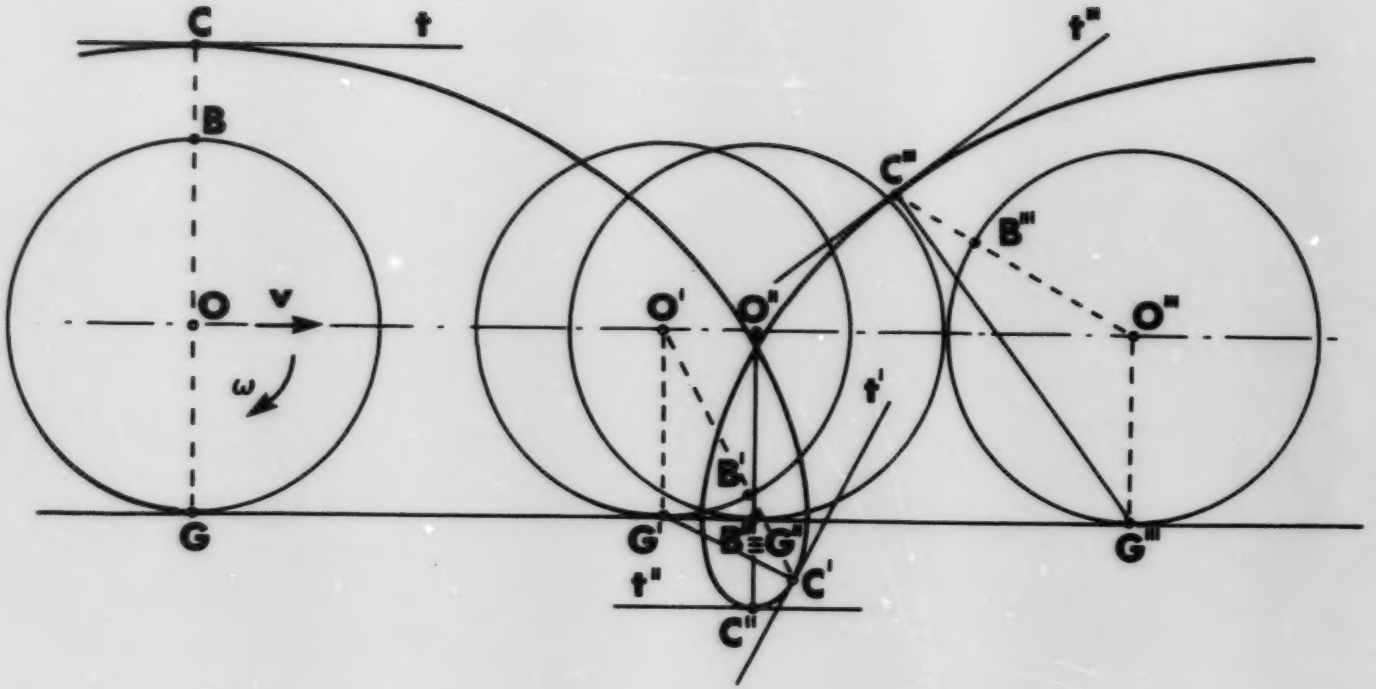


FIGURE 7: Generation of Prolate Cycloid

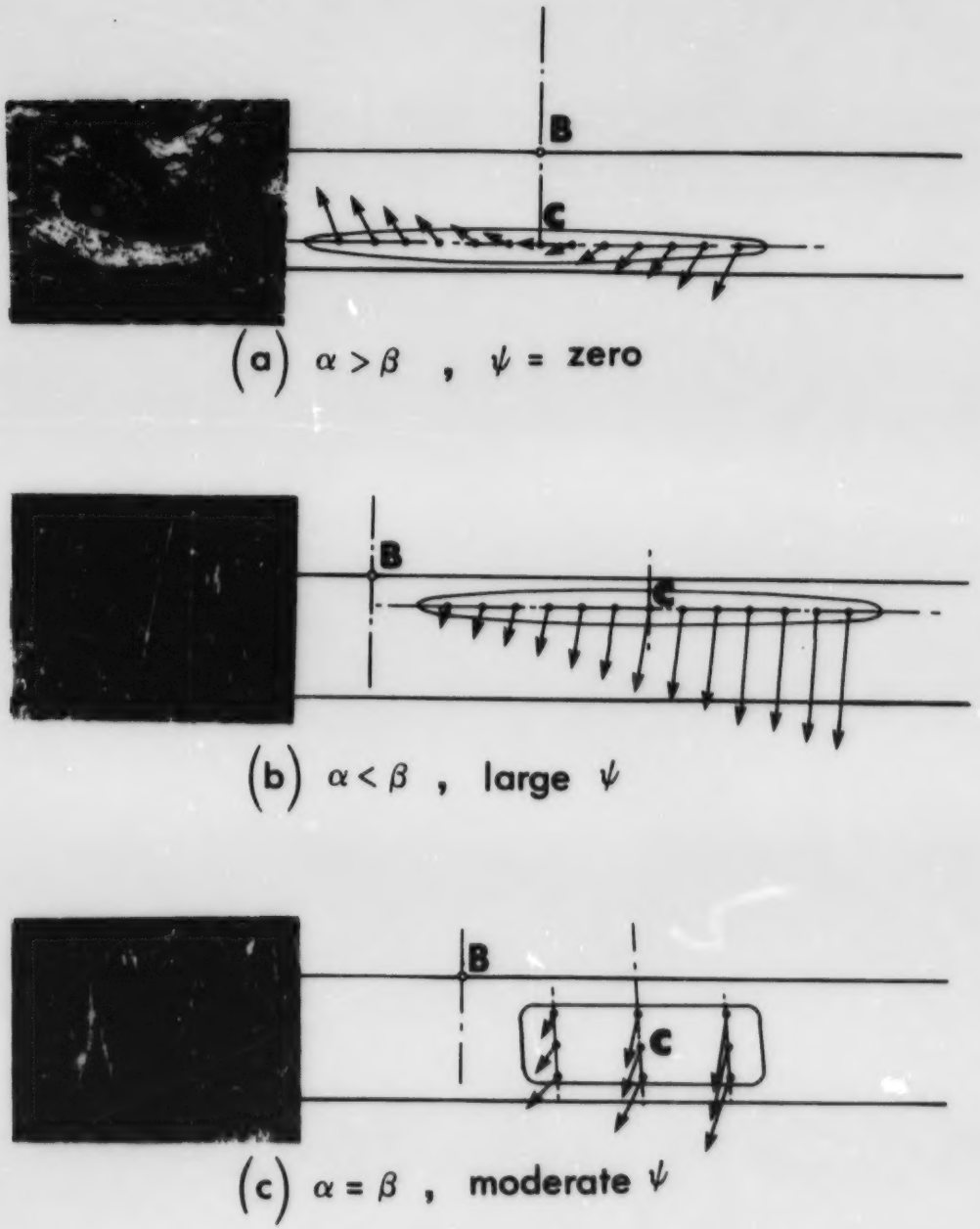


FIGURE 8: Distribution of Slip Vectors Within the Flange Contact

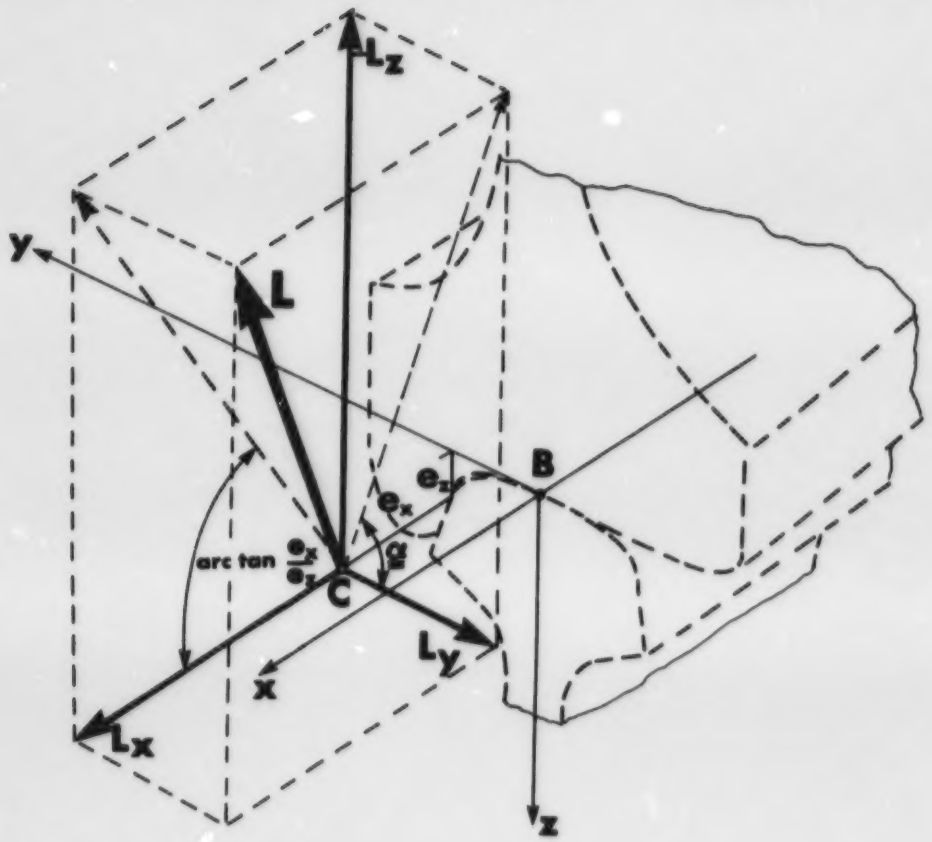


FIGURE 9: Flange Force Vector and Its Orthogonal Components

## REPORT DOCUMENTATION PAGE/PAGE DE DOCUMENTATION DE RAPPORT

| REPORT/RAPPORT | REPORT/RAPPORT |
|---|---|
| 1a TR-WE-42 | NRC 23488<br>1b TDC TP 53463 |
| REPORT SECURITY CLASSIFICATION<br>CLASSIFICATION DE SÉCURITÉ DE RAPPORT<br>2 UNCLASSIFIED | DISTRIBUTION/DIFFUSION<br>3 UNLIMITED |

TITLE/SUBTITLE/TITRE/SOUS-TITRE (CLASSIFICATION)

4 ESTABLISHMENT OF QUANTITATIVE WEAR AND FATIGUE MODEL FOR RAILWAY RAIL SUBJECTED TO HEAVY TRAFFIC CONDITIONS AND DIFFERENT LUBRICATION REGIMES


AUTHOR(S)/AUTEUR(S)

5 J. Kalousek

SERIES/SÉRIE

6 Technical Report

CORPORATE AUTHOR/PERFORMING AGENCY/AUTEUR D'ENTREPRISE/AGENCE D'EXÉCUTION

7 National Research Council Canada (Western Laboratory)
Division of Mechanical Engineering



SPONSORING AGENCY/AGENCE DE SUBVENTION

8 Transport Canada, Transportation Development Centre;
Association of American Railroads, Technical Research Center

| DATE | FILE/DOSSIER | LAB. ORDER<br>COMMANDE DU LAB. | PAGES | DIAGS | REFS |
|---|---|---|---|---|---|
| 9 1984/05 | 10 3793-2-4 | 11 22200 | 12a 50 | 12b 21 | 12c 16 |

NOTES

13


DESCRIPTORS(KEY WORDS)/MOTS-CLÉS

14 Rail Wear, Rail Contact Fatigue, Flaking, Shelly Spots, White Etching Layer, Rail Tribometer, Geometry of Flange Contact


SUMMARY/SOMMAIRE

15 Progress on wear and contact fatigue testing of commercial and experimental rail steels, current status of tribometer development, examination of white etching particles and geometry of flange contact are reported for the Oct. 82 to Sept. 83 period.



ADDRESS/ADRESSE

16 Dr. C. Dayson (Head)
Western Laboratory
3904 West 4th Avenue
Vancouver, B.C. V6R 1P5 (604) 732-4477